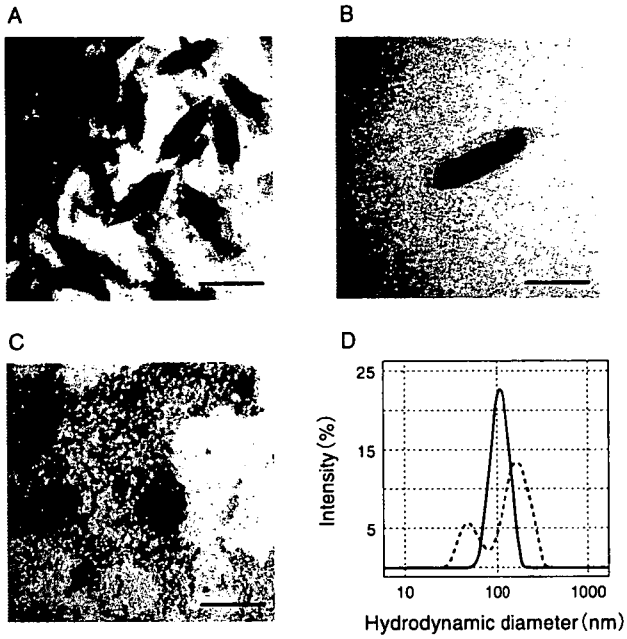

Fig. 1. Characterization of a novel MRI contrast medium.

A-C, Electronmicrographs of iron colloid particles (A), a novel contrast medium (B) and fermoxide (C) was prepared as described in Methods. The bar indicates 40 nm. D, Distribution of hydrodynamic diameter was determined by dynamic light scattering. Solid line: a novel contrast medium, broken line: fermoxide.

Statistical Analysis

Statistical analysis was performed by ANOVA with Bonferroni's modification. The data are presented as the mean ± standard error of the mean. Difference was considered statistically significant when $p<0.05$.

Results

Novel Contrast Agent

We prepared monodispersed iron colloids using a new crystallization technique that we developed[21]. Dynamic light scattering measurements showed that the hydrodynamic diameter was 76.5 nm with narrow single distribution (poly dispersity index: 0.135). Electron microscopy confirmed that they were ellipsoidal particles of homogeneous size (**Fig. 1A**). This technique enabled us to prepare monodispersed iron colloids of any size from 20 to 200 nm in hydrodynamic diameter by changing the aging conditions (data not shown).

The iron colloid was incorporated into a drug deliver system based on a block copolymer of poly (ethylene glycol)-poly (amino acid) by mixing colloids and copolymer at room temperature[17]. The resulting contrast medium had an ellipsoidal-shaped iron core with a lucent envelop of the block copolymer around the core (**Fig. 1B**). The envelope was homogeneous and the thickness was about 10-20 nm. Commercially available iron-based contrast medium (ferumoxide) showed an amorphous mixture of iron and dextran (**Fig. 1C**). Dynamic light scattering measurements showed that the hydrodynamic diameter of the novel contrast medium was 102.4 nm with a polydispersity index of 0.126. Ferumoxide had a similar diameter of 99.4 nm but showed a greater polydispersity index (0.311) (**Fig. 1D**). Relaxivities R1 and R2 of the novel contrast medium at 25℃ in 0.47 T were 1.96 and 2.33 $(mmol/L \cdot sec)^{-1}$, respectively.

T2 Mapping Detected Injured Carotid Artery

To detect small difference in T2 relaxation time between the lesion and the normal tissue, we mapped the T2 relaxation time of the rat injured carotid artery. A proton density-weighted image at echo time of 8 ms and five T2-weighted images at echo times of 12, 16, 20, 40, and 80 ms were obtained at three sites: the uninjured right carotid artery (site 1 in **Fig. 2A** and **Fig. 2B**), injured left carotid artery covered with regenerating endothelial cells (site 2 in **Fig. 2A** and **Fig. 2C**) and injured artery that was not re-endothelialized (site 3 in **Fig. 2A** and **Fig. 2D**). Signal intensities at each echo time showed that the contrast between injured and uninjured arteries increased as echo time increased whereas signal intensity itself decreased (**Fig. 2B, C, D**). MR images at earlier echo times gave clearer images of the tissue, but did not detect differences between injured and uninjured arteries. In contrast, images at later echo times were of poorer quality, but they did detect differences between injured and uninjured arteries (**Fig. 2B, C, D**).

T2 relaxation time of each voxel was calculated based on signal intensities at echo times of 8, 12, 16, 20, 40 and 80 ms by fitting a nonlinear least-squares curve (**Fig. 3E**). A T2 mapping image was reconstructed from the calculated T2 relaxation time of each voxel. This gave a clearer image and better contrast of tissue structure in injured arteries (**Fig. 2F, G, H**). These images corresponded well with the histology of the arteries; an unre-endothelialized site stained with Evans Blue dye had a significantly thicker intima than the re-endothelialized site, and the uninjured artery did not have intimal thickening (**Fig. 2I, J, K**). We also demonstrated that the injured artery had a longer T2 relaxation time than uninjured arteries (50.6 ± 9.5 ms vs 26.9 ± 2.4 ms, $p<0.01$, $n=5$).

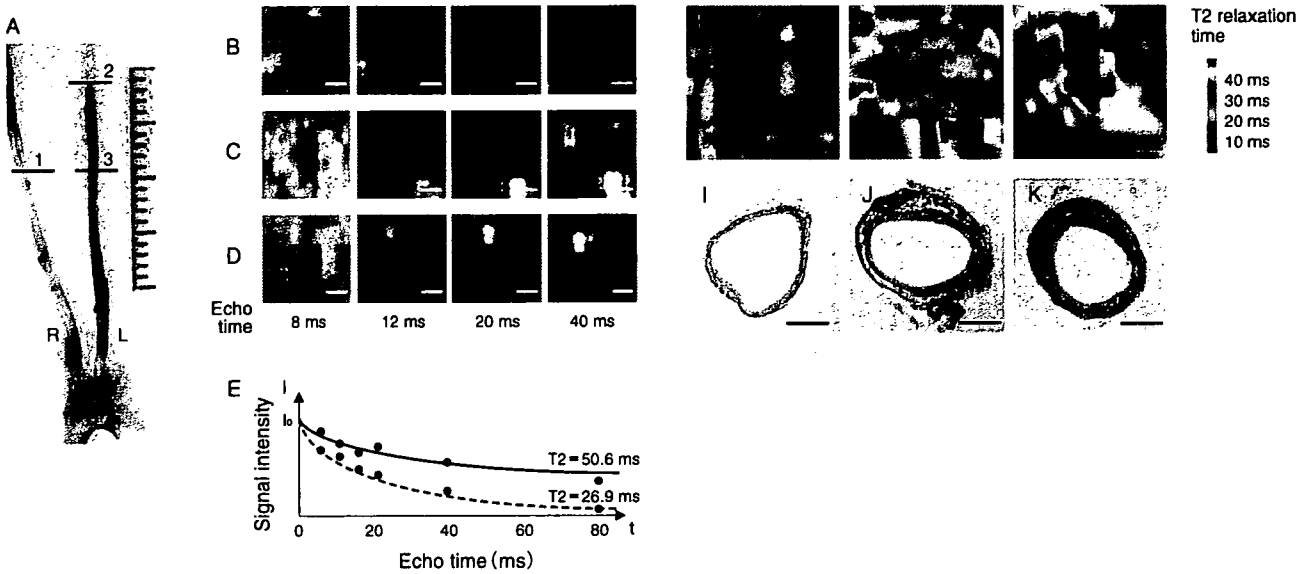

Fig. 2. T2 mapping detected injured carotid artery.

A, left (L) and right (R) carotid arteries indicating the sites of MR imaging and histological sections. The rat was injected with Evans blue dye before sacrifice, and the injured artery without endothelial cells was stained blue. B-D, proton density-weighted image and a series of T2 weighted images of various echo times (TE) of site 1 (B), site 2 (C) and site 3 (D) of panel A are shown. E, non-linear curve square fitting of signal intensities at site 1 (broken line) and site 3 (solid line) at various echo times. T2 relaxation time (T2) was calculated based on signal intensities obtained from five rats by the following equation: $I = I_0 \times \mathrm{Exp}(-t/T2)$ (I: Signal intensity, t: echo time and I_0: I(t=0 ms)).

A Novel Contrast Medium Detected Lesions with Increased Permeability

We then tested whether our novel contrast medium detected increased permeability of macromolecules in injured arteries. Intravenous injection of the contrast medium (0.1 mmol Fe/kg) shortened the T2 relaxation time of a portion of the injured artery and enhanced that part of the artery on T2 mapping image (**Fig. 3A**, middle). This enhancement became apparent as early as one hour after the injection and disappeared by 24 hours (**Fig. 3A**, right). This enhanced lesion corresponded to the lesion with increased permeability that was detected with Evans blue staining (**Fig. 2A**). In contrast, the uninjured artery gave T2 relaxation times identical to those of the surrounding tissue and the contrast medium did not shorten the T2 relaxation time (**Fig. 3B**). Ferumoxide did not enhance any lesions, even when the amount of iron injected was increased 100 times (10 mmol Fe/kg) (data not shown).

To quantitatively analyze this enhancement, we compared T2 relaxation times of 0.3 mm of the luminal side of the injured artery that was not re-endothelialized and the arterial wall between 1.0 and 1.5 mm from the luminal edge of the same site of the artery. T2 relaxation time of the former area significantly decreased one hour after injection and recovered by 24 hours (**Fig. 4A**), where as that of the latter area was not affected by contrast medium (**Fig. 4B**). T2 relaxation time of the uninjured artery was shorter than that of the injured artery and was not affected by contrast medium (**Fig. 4C**).

Fig. 3. A novel contrast medium detected increased permeability of the injured artery.

A rat with injured arteries was injected with a novel contrast medium (0.1 mmol Fe/kg). T2 mapping images were obtained before, 1, 2, 4, and 24 hours after injection. A, injured artery not covered with endothelial cells (site 3 in Fig. 2A). B, uninjured artery (site 1 in Fig. 2A). A representative image of four animals is shown.

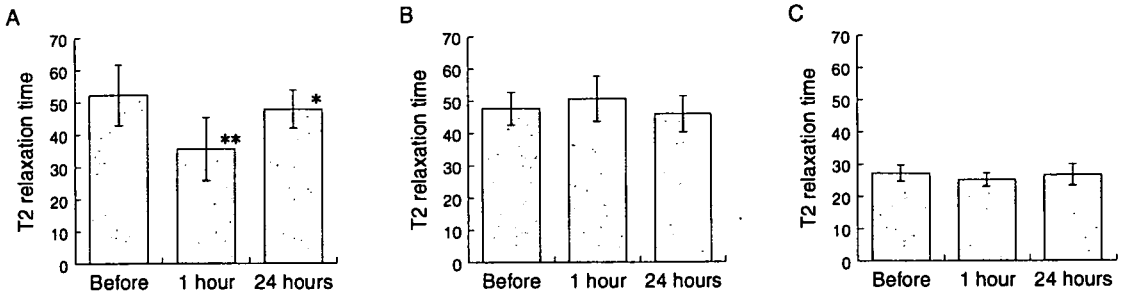

Fig. 4. Quantitative analysis of enhancement by contrast medium.

T2 relaxation times of 0.3 mm of the luminal side of the injured artery that was not re-endothelialized (A), the arterial wall between 1.0 and 1.5 mm from the luminal edge of the same site of the artery (B) and uninjured artery (C) before, 1 hour and 24 hours after injection. Each column represents the mean ± SD of four animals.

Discussion

In this paper, we presented a novel iron MRI contrast medium that was prepared using a block copolymer-based drug delivery system. This contrast medium extravasates and accumulates at the lesion with increased permeability and, in combination with T2 mapping, can detect increased permeability of the injured artery.

Vascular lesions can be detected by MRI with or without contrast media. Plane MRI detects thickened intima of human, rabbit, and rat carotid arteries as well as mouse aorta as medium to high intensity lesions in T2-weighted images. Superparamagnetic iron oxide particles enhance these lesions and give better images. Iron particles accumulate at the lesions by being phagocytosed by macrophages that infiltrate the lesion. We have improved the detection of vascular lesion using two methods: T2 mapping and a novel contrast medium that accumulates in the lesion with increased permeability.

We showed that T2 mapping is useful to detect lesions of the artery. Signal intensity (I) at each echo time (t) is given by the equation: $I = I_0 \times \mathrm{Exp}\ (-t/T2)$, where the T2 relaxation time (T2) is a constant specific for each tissue. Signal intensities decrease as echo time increases; however, the ratio of signal intensities of two sites with different T2 relaxation times or the contrast of the image increases as echo time increases. The quality of T2-weighted images depends on two conflicting factors that vary by echo time. T2 mapping resolves this conflict and gives direct information of T2 relaxation time in tissue. In addition, T2 mapping images have similar characteristics regardless of the equipment manufacturer because T2 relaxation processes are not affected by the intensity of the magnetic field.

T2 mapping images do not necessarily correspond to the anatomical structure of the injured artery as they depicts lesions containing more water than the normal artery. Lesions with higher water content were not limited to the thickened intima but extended to the media and part of the adventitia. T2 mapping images of vascular lesions indicate the extent of tissue edema of the artery followed by injury. Similarly, this technique is expected to sensitively detect lipid-rich atheroma, since the two major factors affecting T2 relaxation times are the tissue content of water and lipid.

Our novel contrast medium has three distinguishing characteristics. First, the particle size is homogeneous. This was possible because we used a new technique to crystallize iron colloids. Any size between 20-200 nm can be prepared and these sizes show monodispersity. It may be possible to clinically estimate the magnitude of increased permeability by using a contrast medium with different particle sizes in the future. Second, our contrast medium has a longer half-life than naked iron colloids in the blood (data not shown). The contrast medium is a stealth nanoparticle[23] that escapes detection and clearance by the reticuloendothelial system of the body, mainly due to its small particle size and minimal surface charge. The longer half-life, together with selective accumulation at the lesion as mentioned below contributes to reduce the amount of medium required to enhance the lesion. Previous studies showed that effective doses of adriamycin could be significantly reduced by incorporating it into the block copolymer-based drug delivery system[20, 24]. This drug delivery system accumulates macromolecules such as iron colloids at lesions by an enhanced permeability retention effect[19], and the increased permeability of macromolecules can be detected with a small amount of contrast medium. In this sense, our contrast medi-

um is quite different from other iron nanoparticles that accumulate at the lesion by phagocytosis[14] because a large amount of other iron nanoparticles are required to detect vascular lesions. Finally, this drug delivery system theoretically accommodates both contrast medium and agent for treatment, therefore enabling us to simultaneously detect and treat vascular lesions[25, 26]. Furthermore, this particle can be modified to deliver agents to the target tissue more precisely[27].

Acknowledgments

This study was support by Special Coordination Funds from the Ministry of Education, Science, Technology, and Culture of Japan to KK and KS. We acknowledge Drs. K. Hanaoka and T. Nagano for measurements of relaxivities, and Nakamura T for conducting transmission electron microscopy. Block copolymer was kindly provided by Dr. I. Nakatomi (Nano Carrier).

References

1) Yuan C, Beach KW, Smith LH Jr., and Hatsukami TS: Measurement of atherosclerotic carotid plaque size in vivo using high resolution magnetic resonance imaging. Circulation, 1998; 98:2666-2671
2) Kaneko E, Skinner MP, Raines EW, Yuan C, Rosenfeld ME, Wight TN, and Ross R: Detection of dissection and remodeling of atherosclerotic lesions in rabbits after balloon angioplasty by magnetic-resonance imaging. Coron Artery Dis, 2000; 11:599-606
3) Fuster V and Kim RJ: Frontiers in cardiovascular magnetic resonance. Circulation, 2005; 112:135-144
4) Fayad ZA, Nahar T, Fallon JT, Goldman M, Aguinaldo JG, Badimon JJ, and Fuster V: In vivo magnetic resonance evaluation of atherosclerotic plaques in the human thoracic aorta: a comparison with transesophageal echocardiography. Circulation, 2000; 101:2503-2509
5) Moody AR, Murphy RE, Morgan PS, Martel AL, Delay GS, Allder S, MacSweeney ST, Tennant WG, Gladman J, Lowe J, and Hunt BJ: Characterization of complicated carotid plaque with magnetic resonance direct thrombus imaging in patients with cerebral ischemia. Circulation, 2003; 107:3047-3052
6) Fayad ZA, Fuster V, Fallon JT, Jayasundera T, Worthley SG, Helft G, Aguinaldo JG, Badimon JJ, and Sharma SK: Noninvasive in vivo human coronary artery lumen and wall imaging using black-blood magnetic resonance imaging. Circulation, 2000; 102:506-510
7) Anumula S, Song HK, Wright AC, and Wehrli FW: High-resolution black-blood MRI of the carotid vessel wall using phased-array coils at 1.5 and 3 Tesla. Acad Radiol, 2005; 12:1521-1526
8) Donald W, McRobbie EAM, Martin J Graves, and Martin R: MRI from Picture to Proton, pp135-163, Cambridge University Press, 2002
9) Rugg-Gunn FJ, Boulby PA, Symms MR, Barker GJ, and Duncan JS: Whole-brain T2 mapping demonstrates occult abnormalities in focal epilepsy. Neurology, 2005; 64:318-325
10) Mosher TJ, Collins CM, Smith HE, Moser LE, Sivarajah RT, Dardzinski BJ, and Smith MB: Effect of gender on in vivo cartilage magnetic resonance imaging T2 mapping, 2004; 19:323-328
11) Watrin-Pinzano A, Ruaud JP, Olivier P, Grossin L, Gonord P, Blum A, Netter P, Guillot G, Gillet P, and Loeuille D: Effect of proteoglycan depletion on T2 mapping in rat patellar cartilage. Radiology, 2005; 234:162-170
12) Wood JC, Enriquez C, Ghugre N, Tyzka JM, Carson S, Nelson MD, and Coates TD: MRI R2 and R2* mapping accurately estimates hepatic iron concentration in transfusion-dependent thalassemia and sickle cell disease patients. Blood, 2005; 106:1460-1465
13) Ruehm SG, Corot C, Vogt P, Kolb S, and Debatin JF: Magnetic resonance imaging of atherosclerotic plaque with ultrasmall superparamagnetic particles of iron oxide in hyperlipidemic rabbits. Circulation, 2001; 103:415-422
14) Trivedi RA, U-King-Im JM, Graves MJ, Cross JJ, Horsley J, Goddard MJ, Skepper JN, Quartey G, Warburton E, Joubert I, Wang L, Kirkpatrick PJ, Brown J, and Gillard JH: In vivo detection of macrophages in human carotid atheroma: temporal dependence of ultrasmall superparamagnetic particles of iron oxide-enhanced MRI. Stroke, 2004; 35:1631-1635
15) Barkhausen J, Ebert W, Heyer C, Debatin JF, and Weinmann HJ: Detection of atherosclerotic plaque with Gadofluorine-enhanced magnetic resonance imaging. Circulation, 2003; 108:605-609
16) Yamamoto T, Ikuta K, Oi K, Abe K, Uwatoku T, Hyodo F, Murata M, Shigetani N, Yoshimitsu K, Shimokawa H, Utsumi H, and Katayama Y: In vivo MR detection of vascular endothelial injury using a new class of MRI contrast agent. Bioorg Med Chem Lett, 2004; 14:2787-2790
17) Kataoka K, Yokoyama M, Okano T, and Sakurai Y: Block copolymer micelles as vehicles for drug delivery. J Control Release, 1993; 24:119-132
18) Otsuka H, Nagasaki Y, and Kataoka K: PEGylated nanoparticles for biological and pharmaceutical applications. Adv Drug Deliv Rev, 2003; 55:403-419
19) Yokoyama M, Fukushima S, Uehara R, Okamoto K, Kataoka K, Sakurai Y, and Okano T: Characterization of physical entrapment and chemical conjugation of adriamycin in polymeric micelles and their design for in vivo delivery to a solid tumor. J Control Release, 1998; 50:79-92
20) Yokoyama M, Okano T, Sakurai Y, Fukushima S, Okamoto K, and Kataoka K: Selective delivery of adriamycin to a solid tumor using a polymeric micelle carrier system. J Drug Target, 1999; 7:171-186
21) Kataoka K, Imai Y, and Kumagai M: Process for producing iron colloid, and iron-colloid-bearing polymer micelle. US patent pending, 2005
22) Reidy MA, Clowes AW, and Schwartz SM: Endothelial regeneration. V. Inhibition of endothelial regrowth in arteries of rat and rabbit. Lab Invest, 1983; 49:569-575

23) Fang C, Shi B, Pei YY, Hong MH, Wu J, and Chen HZ: In vivo tumor targeting of tumor necrosis factor-alpha-loaded stealth nanoparticles: Effect of MePEG molecular weight and particle size. Eur J Pharm Sci, 2006; 27:27-36
24) Yokoyama M, Okano T, Sakurai Y, Ekimoto H, Shibazaki C, and Kataoka K: Toxicity and antitumor activity against solid tumors of micelle-forming polymeric anticancer drug and its extremely long circulation in blood. Cancer Res, 1991; 51:3229-3236
25) Shiba H, Okamoto T, Futagawa Y, Ohashi T, and Eto Y: Efficient and cancer-selective gene transfer to hepatocellular carcinoma in a rat using adenovirus vector with iodized oil esters. Cancer Gene Ther, 2001; 8:713-718
26) Uwatoku T, Shimokawa H, Abe K, Matsumoto Y, Hattori T, Oi K, Matsuda T, Kataoka K, and Takeshita A: Application of nanoparticle technology for the prevention of restenosis after balloon injury in rats. Circ Res, 2003; 92:62-69
27) Nishiyama N, Iriyama A, Jang WD, Miyata K, Itaka K, Inoue Y, Takahashi H, Yanagi Y, Tamaki Y, Koyama H, and Kataoka K: Light-induced gene transfer from packaged DNA enveloped in a dendrimeric photosensitizer. Nat Mater, 2005; 4:934-941

A Facile Synthesis of Azido-Terminated Heterobifunctional Poly(ethylene glycol)s for "Click" Conjugation

Shigehiro Hiki[†] and Kazunori Kataoka*[,†,‡,§]

Department of Materials Engineering, Graduate School of Engineering, and Center for NanoBio Integration, The University of Tokyo, 7-3-1 Hongo, Bunkyo-ku, Tokyo 113-8656, Japan, Core Research Program for Evolutional Science and Technology (CREST), Japan Science and Technology Agency (JST), Tokyo, Japan, and Center for Disease Biology and Integrative Medicine, Graduate School of Medicine, The University of Tokyo, 7-3-1 Hongo, Bunkyo-ku, Tokyo 113-0033, Japan. Received April 27, 2007; Revised Manuscript Received July 26, 2007

New azido-terminated heterobifunctional poly(ethylene glycol) (PEG) derivatives having primary amine and carboxyl end groups, (Azide-PEG-NH_2 and Azide-PEG-COOH, respectively) were synthesized with high efficiency. An α-allyl-ω-hydroxyl PEG was prepared as the first step to Azide-PEG-X (X = NH_2 and COOH) through the ring-opening polymerization of ethylene oxide (EO) with allyl alcohol as an initiator, followed by two-step modification of the hydroxyl end to an azido group. To introduce primary amino or carboxyl functional groups, amination and carboxylation reactions of the allyl terminal ends was then conducted by a radical addition of thiol compounds. Molecular functionalities of both ends of the PEG derivatives thus prepared were characterized by ^1H, ^{13}C NMR, and MALDI-TOF MS spectra, validating that the reaction proceeded quantitatively. The terminal azido functionality is available to conjugate various ligands with an alkyne group through the 1,3-dipolar cycloaddition reaction condition ("click chemistry").

INTRODUCTION

Poly(ethylene glycol) (PEG) conjugation chemistry, termed "PEGylation", has widely been used for the modification of biomolecules such as peptides, proteins, and enzymes (*1–3*), as well as of nanocarriers for drug delivery systems (DDS) such as liposomes and nanoparticles (*4, 5*). The advantages of PEGylation include the improvement of pharmaceutical and pharmacological properties, e.g., increased water solubility and circulatory half-life in vivo, the reduced antigenicity and immunogenicity, and the tolerance of biomolecules against degradation (*1–3*). Actually, several PEG-conjugated proteins have already been available as clinical therapeutics (*6*). Methoxy-terminated monofunctionalized PEG derivatives have mainly been used in these systems. Of further interest from the viewpoint of constructing multifunctionalized biopharmaceutics with PEGylation is the introduction of reactive groups at the α-chain end of PEG to prepare α,ω-heterobifunctional derivatives (heterobifunctional PEG). Heterobifunctional PEG may be useful to install ligands and probes at the distal end of PEGylated liposomes (*7*), polymeric micelles (*8*), synthetic polymers (*9*), and metallic colloids (*10*). So far, several types of heterobifunctional PEG derivatives with reactive groups, such as aldehyde, primary amine, mercapto, and maleimide, have been developed to install a variety of ligands (*8, 11–17*). Nevertheless, to expand the heterobioconjugation through PEG linker into a various combination of ligands and substrates, further improvement in the design of heterobifunctional PEG, particularly from the viewpoint of versatility, is crucial.

Generally, several features such as high yields, chemoselectivity, and the mild reaction condition in aqueous media are indispensable for the bioconjugation. In this regard, the 1,3-dipolar cycloaddition reaction between alkyne and organic azides, yielding the corresponding 1,2,3-triazoles in the mild aqueous condition, has recently received considerable attention in wide areas of chemistry (*18–20*) and has been recognized as particularly useful in the field of bioconjugate chemistry (*21–24*). This Cu(I)-catalyzed 1,3-dipolar cycloaddition reaction (termed "click chemistry") is highly chemoselective and can be performed under mild conditions in aqueous buffers with wide range of pH values. Therefore, the combination of heterobifunctional PEGs with "click chemistry" is a promising approach for bioconjugation (*25*). Indeed, the introduction of biological ligands by "click chemistry" onto the liposomal surface (*26*) and the Au nanoparticle surface (*27*) through the heterobifunctional oligo(ethylene glycol) spacers was recently reported, indicating the high utility of "click"-based bioconjugation.

Nevertheless, little attention has been placed on the novel and versatile method to prepare the azido-terminated heterobifunctional PEGs with a wide range of molecular weight useful for "click"-based bioconjugation. Although, azido-containing oligo(ethylene glycol) derivatives (e.g., N_3-$(CH_2CH_2O)_2$-$CH_2CH_2NH_2$) have been commercialized (*28*), the azido-terminated heterobifunctional PEGs having high molecular weight useful in the bioconjugate chemistry field are not yet available.

Here, we wish to communicate the new synthetic route of azido-terminated heterobifunctional PEGs possessing primary amino and carboxyl groups (Azide-PEG-NH_2 and Azide-PEG-COOH, respectively) with controlled molecular weight through the ring-opening polymerization of ethylene oxide from allyl alcohol as an initiator followed by a quantitative modification of α- and ω-end groups (Scheme 1).

EXPERIMENTAL PROCEDURES

Materials. Ethylene oxide (EO; Sumitomo Seika Chemical, Japan) was dried over calcium hydride and distilled under an argon atmosphere. Allyl alcohol, tetrahydrofuran (THF), *N,N-*

* To whom corresponding should be addressed. Professor Kazunori Kataoka. Tel: +81-3-5841-7138. Fax: +81-3-5841-7139. E-mail: kataoka@bmw.t.u-tokyo.ac.jp.

† Graduate School of Engineering, The University of Tokyo, and CREST.

‡ Graduate School of Medicine, The University of Tokyo.

§ Center for NanoBio Integration, The University of Tokyo.

10.1021/bc700152j CCC: $37.00 © 2007 American Chemical Society
Published on Web 10/25/2007

Scheme 1. Synthetic Route to α-Amino-ω-azido-PEG (3) and α-Carboxy-ω-azide-PEG (4)

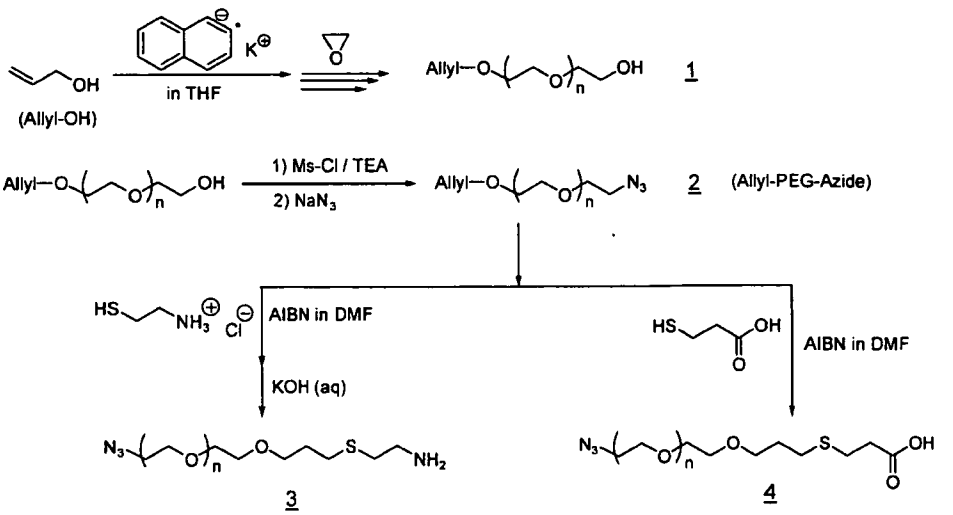

dimethylformamide (DMF), triethylamine, 2,2′-azobisisobutyronitrile (AIBN), and methanesulfonyl chloride were purchased from Wako Pure Chemical Industries, Ltd., (Osaka, Japan) and purified by conventional methods. Potassium naphthalene was prepared as a THF solution according to a previous paper (*29*), whose concentration was determined by titration. 2-Aminoethanethiol hydrochloride, mercaptopropionic acid, sodium azide, and other reagents were used as received.

Synthesis of α-Allyl-ω-hydroxyl PEG (1). Allyl alcohol (2.3 mmol, 135 μL) and potassium naphthalene (2 mmol) in 6.6 mL of THF were added to dry THF (75 mL) in a 200 mL flask equipped with a three-way stopcock under argon atmosphere to form potassium allyl alcoholate as an initiator. After stirring for 10 min, liquid EO (302 mmol, 13.3 g) was added to the solution via a cooled syringe. The mixture was allowed to react for 2 days at 25 °C followed by pouring into diethyl ether to precipitate the polymer. The recovered polymer was dried in vacuo and then freeze-dried from benzene. The yield of obtained polymer after purification was 91% (12.1 g). GPC: Number-average molecular weight (M_n) = 5500, M_w/M_n = 1.03. ^{1}H NMR (300 MHz, $CDCl_3$, δ in ppm): 3.63 (m, O-(C*H*$_2$)$_2$-O), 4.02 (d, C*H*$_2$ of allyl group), 5.17–5.30 (dd, C*H*$_2$ of allyl group), 5.87–5.96 (m, C*H* of allyl group).

Synthesis of α-Allyl-ω-azide PEG (2). The azide end group was introduced by the mesylation of the hydroxyl terminus and subsequent substitution with sodium azide, referring to the literature methods (*30*).

Freeze-dried polymer **1** (Allyl-PEG-OH) (2.20 g, 0.40 mmol) from benzene was dissolved in anhydrous THF (15 mL) followed by triethylamine (162 mg, 1.60 mmol) addition. The mixture was then added to a solution of methanesulfonyl chloride (160 mg, 1.40 mmol) in THF (8 mL) under Ar stream, and stirred overnight at room temperature. After the reaction, THF was partially evaporated under reduced pressure. The residue was redissolved in water (40 mL) and extracted with dichloromethane (5 × 100 mL). The organic layers were combined and dried over Na_2SO_4. After filtration and concentration, the polymer was recovered by precipitation into ether and dried in vacuo, yielding a white solid.

This mesylated polymer (620 mg, 0.113 mmol) was dissolved in DMF (12 mL), followed by sodium azide (521 mg, 8.01 mmol) addition, and was stirred for 2 days at 30 °C. Dichloromethane (100 mL) was then added, and the reaction mixture was washed five times with water and brine. The organic layer was dried over Na_2SO_4, filtered, concentrated, and then reprecipitated into ether. The recovered polymer was freeze-dried from benzene (508 mg, 82%). ^{1}H NMR (300 MHz, $CDCl_3$, δ in ppm): 3.46 (t, CH_2-C*H*$_2$-N_3), 3.63 (s, O-(C*H*$_2$)$_2$-O), 4.02 (d, C*H*$_2$ of allyl group), 5.17–5.30 (dd, C*H*$_2$ of allyl group), 5.87–5.96 (m, C*H* of allyl group).

Synthesis of α-Amino-ω-azide PEG (3). Amination of the allyl terminus of polymer **2** was conducted by the radical addition reaction of 2-aminoethanethiol hydrochloride (*31*). Polymer **2** (Allyl-PEG-azide, 502 mg, 0.091 mmol) was freeze-dried from benzene and mixed with the solution in DMF (5 mL) containing 213 mg of 2-aminoethanethiol hydrochloride (1.87 mmol, 20 equiv) and 15 mg of AIBN (0.091 mmol, 1 equiv). The reaction mixture was stirred at 65 °C for 24 h under argon atmosphere. The polymer was precipitated twice in a large excess of ether. The resulting white product was dissolved into methanol, and 5.1 mg (1 equiv) of potassium hydroxide dissolved in water was added. The mixture was stirred for approximately 4 h. Then, methanol was partially evaporated and diluted with water (30 mL), and extracted by dichloromethane (5 × 80 mL). The combined organic layer was dried over Na_2SO_4, filtered, and concentrated to 1/100 of the initial volume. The polymer was reprecipitated from an excess volume of ether and freeze-dried from benzene to lead to a white powder (397 mg, yield = 79%).

Synthesis of α-Carboxy-ω-azide PEG (4). The carboxylation reaction of allyl terminus of polymer **2** was performed in the same manner as described above for the preparation of polymer **3**. Typically, 409 mg of Allyl-PEG-azide, in 4 mL of DMF, was reacted with 159 mg of 3-mercaptopropionic acid (1.50 mmol, 20 equiv) in the presence of 12.2 mg of AIBN (1 equiv). After the reaction, the solution was precipitated into ether twice, and polymer **4** was obtained as a white powder (317 mg, yield = 77%).

Polymer Analysis. ^{1}H and ^{13}C NMR spectra were recorded on a JEOL JNM-AL 300 spectrometer (JEOL, Tokyo, Japan) at 300 and 75.45 MHz, respectively. Chemical shifts are reported in parts per million (ppm) downfield from tetramethylsilane. Number-average molecular weight (M_n) and molecular weight distribution (M_w/M_n) were determined using a GPC (TOSOH HLC-8220) system equipped with two TSK gel columns (G4000HHR and G3000HHR) and an internal refractive index (RI) detector. Columns were eluted with DMF containing lithium chloride (10 mM) at a flow rate of 0.8 mL/min and temperature of 40 °C. Molecular weights were calibrated with poly(ethylene glycol) standards (Polymer Laboratories, Ltd., UK). MALDI-TOF-MS spectra were recorded using Bruker

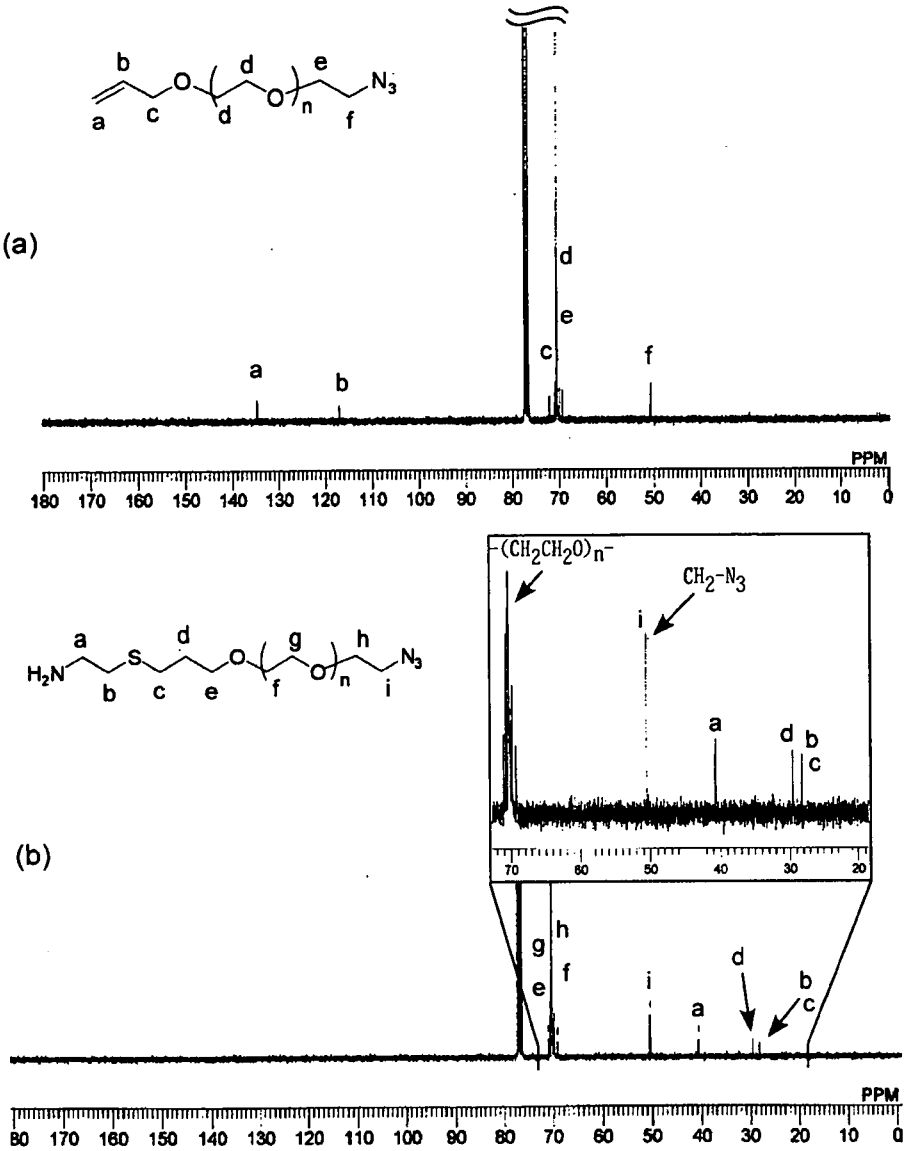

Figure 1. (a) ^{13}C NMR spectrum of Allyl-PEG-Azide ($CDCl_3$ at 20 °C). (b) ^{13}C NMR spectrum of Azide-PEG-NH_2 ($CDCl_3$ at 20 °C).

REFLEX III. α-Cyano-4-hydroxycinnamic acid (CHCA) was used as the matrix for the ionization operated in the reflection mode.

RESULTS AND DISCUSSION

There are several reports on the preparation of oligo(ethylene glycol)s having azido and amino groups from homotelechelic oligo(ethylene glycol)s as the starting materials (*32, 33*). Nevertheless, the synthetic methods involve several complicated reactions as well as separation steps such as chromatographic isolation due to the difficulty of selective monoprotection of the hydroxyl termini. Thus, the application of these synthetic approaches of end-group modification is not expedient for a large-scale synthesis of heterobifunctional PEGs having high molecular weight, giving an impetus to develop a novel synthetic route to the azide-functionalized heterobifunctional PEG with quantitative yields and high specificity under mild reaction conditions.

In this study, allyl alcoholate was selected as an initiator for anionic polymerization of EO, because the allyl end group of the PEG chain allows several kinds of chemical modifications such as addition reactions. To prepare α-allyl-ω-hydroxyl PEG (**1**), the anionic polymerization of EO initiated with potassium allyl alcoholate was carried out in THF solution for 48 h. After precipitation into ether, the product was obtained as white powder. The MW of the polymer **1** (Allyl-PEG-OH) determined from GPC [M_n(GPC) 5500] was close to that from the initial monomer/initiator ratio [M_n(calcd) 5780], indicating an effective initiation efficiency of potassium allyl alcoholate without detrimental side reactions.

α-Allyl-ω-azide PEG (**2**) was obtained through the two-step modification, the mesylation and the subsequent substitution by sodium azide, of hydroxyl function as described in the Experimental Procedures. In the ^{13}C NMR spectrum (Figure 1a), the signals of the carbons of the allyl group are detected at δ 134.7 ppm (a), 117.0 ppm (b), and 72.1 ppm (c), respectively. In addition to these signals, the methylene unit adjacent to the azido group ($CH_2\underline{C}H_2N_3$) was observed at 50.5 ppm (f). Moreover, no signal of the methylene carbon adjacent to the hydroxyl terminus ($CH_2\underline{C}H_2OH$ δ = 61.5 ppm) (*34*) was detected.

Figure 2a shows the MALDI-TOF MS spectra of α-allyl-ω-azide PEG (**2**). In this analysis, although the major peaks of the polymer were detected as the species derived from loss of N_2 from azido group which ascribed to fragmentation due to

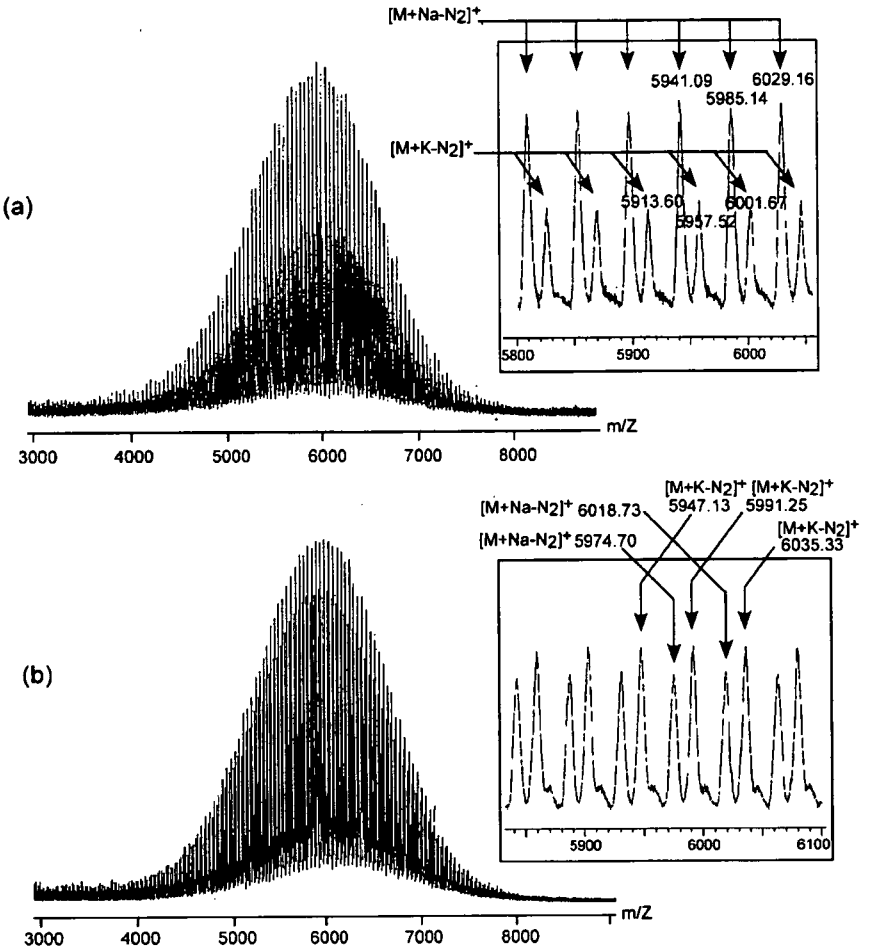

Figure 2. MALDI-TOF Mass Spectrum of Allyl-PEG-Azide (a) and Azide-PEG-NH_2 (b).

the higher laser power during MALDI experiment (*35*), only parent ions of each polymer molecule as planned are observed, without the signal of the side reaction product. From the expanded view of the spectrum in Figure 2a, the mass of the products appears to be around 5900 (M_n = 5670; M_w/M_n = 1.03), which is in a good accordance with the GPC results (M_n = 5500). These data demonstrated that α-allyl-ω-hydroxyl PEG (**1**) was successfully transformed to α-allyl-ω-azide PEG (**2**). Note that there was a report on the chain degradation of tosylate-activated PEG derivatives (*36*). Nevertheless, no sign of degradation was found in the present case of mesylate-activated PEG samples by MALDI-TOF MS spectroscopy, indicating that essentially no degradation of PEG occurred in the activation route via mesylation.

To prepare α-amino-ω-azide PEG, the radical addition reaction of 2-aminoethanethiol hydrochloride to an allyl end group of polymer (**2**) was examined according to the previous method with a slight modification (*31*). The reaction was carried out under the varying ratios of [allyl-PEG-azide]$_0$/[$HSCH_2CH_2NH_3^+Cl^-$]$_0$/[AIBN]$_0$ (=1/5/1, 1/7.5/1, 1/10/1, and 1/20/1 mol equiv) in DMF at 65 °C. The resulting polymer was precipitated twice in ether in order to remove excess of reagents. After the subsequent aqueous workup with potassium hydroxide, the amino-terminated PEG sample was obtained (Scheme 1). The ^{1}H NMR spectrum of the polymer obtained at the conditions of [allyl-PEG-azide]$_0$/[$HSCH_2CH_2NH_3^+Cl^-$]$_0$/[AIBN]$_0$ = 1/10/1 and 1/20/1 revealed the complete disappearance of the signals assigned to the allyl protons at 4.02 (CH_2=CHC$\underline{H_2}$), 5.17–5.30 (C$\underline{H_2}$=$CHCH_2$), and 5.87–5.96 ppm (CH_2=C$\underline{H}CH_2$). Concomitantly, the new signals were clearly observed at 1.82 ($CH_2C\underline{H_2}CH_2S$), 2.60 ($SC\underline{H_2}CH_2NH_2$), 2.62 ($C\underline{H_2}SCH_2CH_2NH_2$), and 2.86 ppm ($CH_2SCH_2C\underline{H_2}NH_2$) corresponding to the resulting structure via the radical addition of 2-aminoethanethiol to allyl group. A decreased ratio of thiol compound in the initial reaction mixture to less than 10 equiv ([allyl-PEG-azide]$_0$/[$HSCH_2CH_2NH_3^+Cl^-$]$_0$/[AIBN]$_0$ = 1/5/1 and 1/7.5/1) resulted in the incomplete amination judged from the observation of the remaining ally protons in the ^{1}H NMR spectra of the obtained polymer samples, suggesting that 10 mol excess equiv of thiol group may be required for the complete amination of allyl group settled at the PEG chin end. No prohibitive effect was observed even at 20 equiv of thiol to allyl groups. In the ^{13}C NMR spectra of the sample obtained at [allyl-PEG-azide]$_0$/[$HSCH_2CH_2NH_3^+Cl^-$]$_0$/[AIBN]$_0$ = 1/20/1 (Figure 1b), no carbon signal corresponding to allyl function remained. The signals detected around δ 40.7 (a), 29.6 (d), and 28.4 ppm (c,d) can be assigned to the $\underline{C}H_2NH_2$, $CH_2\underline{C}H_2CH_2S$, and $CH_2CH_2\underline{C}H_2S\underline{C}H_2$ of the end groups, respectively. Note that no side reaction of the azido group such as a radical scavenging and a subsequent decomposition with denitrogenation occurred, because the signal corresponding to the azido group was detected as intact.

The quantitative conversion of the end allyl group to the primary amino group was also monitored by the MALDI-TOF MS analysis. Figure 2b shows the MALDI-TOF MS spectrum of the reaction product after the radical addition reaction of 2-aminoethanethiol hydrochloride ([allyl-PEG-azide]$_0$/[$HSCH_2CH_2NH_3^+Cl^-$]$_0$/[AIBN]$_0$ = 1/20/1). As mentioned above, the mass distribution of the obtained polymer after the radical addition was the same as that before the reaction, indicating the occurrence of no side reaction. The major series of the molecular masses of the product is expressed in the following equation.

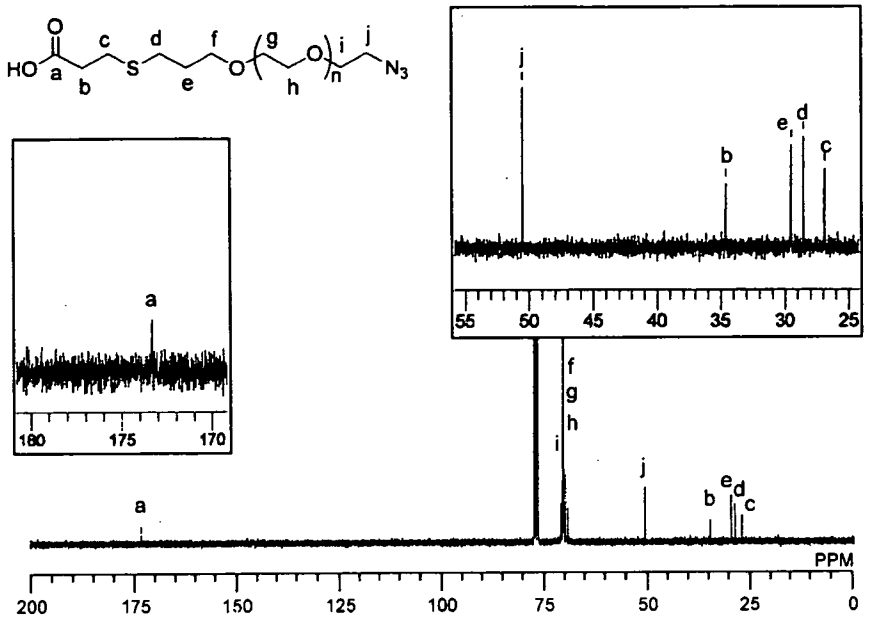

Figure 3. ^{13}C NMR spectrum of Azide-PEG-COOH ($CDCl_3$ at 23 °C).

MW_{MS} = 44.053n (EO) + 70.07 (Azide) + 134.22 ($OCH_2CH_2CH_2SCH_2CH_2NH_2$) + 22.99 (sodium).

These results strongly supported the statement that the novel heterobifunctional PEG possessing an azido group at one end and a primary amino group at the other end was quantitatively prepared.

To demonstrate the versatility of this synthetic route with azido-containing PEG, the carboxylation of α-allyl-ω-azide PEG (**2**) was examined under the same conditions as the amination reaction ([allyl-PEG-azide]$_0$/[$HSCH_2CH_2COOH$]$_0$/[AIBN]$_0$ = 1/20/1). From the ^1H NMR analysis of the resultant polymer, the signals assigned to the allyl group completely disappeared after the reaction, while the methylene protons of the 3-mercaptoacetic acid unit were clearly observed at 1.84 ($CH_2\underline{CH_2}CH_2S$), 2.60 ($SC\underline{H_2}CH_2COOH$), 2.62 ($C\underline{H_2}SCH_2CH_2COOH$), and 2.79 ppm ($CH_2SCH_2C\underline{H_2}COOH$), respectively. In addition, the structure of the resulting polymer after the carboxylation reaction was confirmed by ^{13}C NMR. The corresponding carbon signals of the terminal groups appeared at δ 173.0 ((a) $CH_2\underline{C}OOH$), 50.4; ((j) $\underline{C}H_2N_3$), 34.5; ((b) $\underline{C}H_2COOH$), 29.6; ((e) $CH_2\underline{C}H_2CH_2S$), 28.5; ((d) $CH_2CH_2\underline{C}H_2S$), and 26.9; ((c) $S\underline{C}H_2CH_2COOH$) ppm, respectively, and no signal corresponding to allyl group was detected (Figure 3). These results indicate the successful preparation of heterobifunctional PEG possessing azido and carboxyl groups at the chain ends.

In conclusion, the facile and quantitative synthesis of azido-containing heterobifunctional PEGs via EO polymerization was demonstrated in this study. These azido-containing PEGs can be used to Cu(I)-catalyzed 1,3-dipolar cycloaddition reaction (click chemistry) to introduce versatile biofunctional ligands into the azido terminus, and are thus relevant to a wide range of applications in the field of bioconjugate chemistry. We focused here on the PEG with MW of 5000 because of its versatility in bioconjugate applications, including liposome modification, polymeric micelle formation, and protein conjugation. Basically, chemistry developed here may be applicable to PEG with even higher MW, because the reaction scheme may not be directly influenced by the MW. Nevertheless, the quantitative conversion is still in an issue for the higher MW PEG due to the limited availability of the chain end possibly buried in the coil of PEG strands. We feel that this issue may be better addressed in a future study directly focusing on the reactivity of the allyl group located at the chain end of PEG with different molecular weights.

ACKNOWLEDGMENT

This work was supported by the Core Research for Evolutional Science and Technology (CREST) from the Japan Science and Technology Agency (JST). The authors thank Dr. Darin Y. Furgeson, University of Wisconsin, for his linguistic review of the manuscript.

LITERATURE CITED

(1) Harris, J. M., Ed. (1992) *Poly(ethylene glycol) Chemistry: Biotechnical and Biomedical Applications*, Plenum Press, New York.

(2) Roberts, M. J., Bentley, M. D., and Harris, J. M. (2002) Chemistry for peptide and protein PEGylation. *Adv. Drug Delivery Rev. 54*, 459–476.

(3) Nucci, M. L., Shorr, R., and Abuchowski, A. (1991) The therapeutic value of poly(ethylene glycol) modified proteins. *Adv. Drug Delivery Rev. 6*, 133–151, and references therein.

(4) Gabizon, A., Goren, D., Horowitz, A. T., Tzemach, D., Lossos, A., and Siegal, T. (1997) Long-circulating liposomes for drug delivery in cancer therapy: a review of biodistribution studies in tumor-bearing animals. *Adv. Drug Delivery Rev. 24*, 337–344.

(5) Kataoka, K., Harada, A., and Nagasaki, Y. (2001) Block copolymer micelles for drug delivery: design, characterization and biological significance. *Adv. Drug Delivery Rev. 47*, 113–131.

(6) Duncan, R. (2003) The drawing era of polymer therapeutics. *Nat. Rev. Drug Discovery 2*, 347–360.

(7) Zalipsky, S., Gittelman, J., Mullah, N., Qazen, M. M., and Harding, J. (1998) *Biologically active ligand-bearing polymer-grafted liposomes, Targeting of Drugs 6: Strategies for Stealth Therapeutic Systems*, pp 131–139, Plenum, New York.

(8) Jule, E., Nagasaki, Y., and Kataoka, K. (2002) Surface plasmon resonance study on the interaction between lactose-installed poly(ethylene glycol)-poly(D,L-lactide) block copolymer micelles and lectins immobilized on a gold surface. *Langmuir 18*, 10334–10339.

(9) Ogris, M., Walker, G., Blessing, T., Kircheis, R., Wolschekd, M., and Wagner, E. (2003) Tumor-targeted gene therapy: strategies for the preparation of ligand-polyethylene glycol-polyethylenimine/DNA complexes. *J. Controlled Release 91*, 173–181.

(10) Popielarski, S. R., Pun, S. H., and Davis, M. E. (2005) A nanoparticle-based model delivery system to guide the rational design of gene delivery to the liver. 1. Synthesis and characterization. *Bioconjugate Chem. 16*, 1063–1070.

(11) Nagasaki, Y., Kutsuna, T., Iijima, M., Kato, M., and Kataoka, K. (1995) Formyl-ended heterobifunctional poly(ethylene oxide): Synthesis of poly(ethylene oxide) with a formyl group at one end and a hydroxyl group at the other end. *Bioconjugate Chem. 6*, 231–233.

(12) Yokoyama, M., Okano, T., Sakurai, Y., Kikuchi, A., Ohsako, N., Nagasaki, Y., and Kataoka, K. (1992) Synthesis of poly-(ethylene oxide) with heterobifunctional reactive groups at its terminals by an anionic initiator. *Bioconjugate Chem. 3*, 275–276.

(13) Nagasaki, Y., Iijima, M., Kato, M., and Kataoka, K. (1995) Primary amino-terminal heterobifunctional poly(ethylene oxide). Facile synthesis of poly(ethylene oxide) with a primary amino group at one end and a hydroxyl group at the other end. *Bioconjugate Chem. 6*, 702–704.

(14) Akiyama, Y., Otsuka, H., Nagasaki, Y., Kato, M., and Kataoka, K. (2000) Selective synthesis of heterobifunctional poly(ethylene glycol) derivatives containing both mercapto and acetal terminals. *Bioconjugate Chem. 11*, 947–950.

(15) Gao, X., Tao, W., Lu, W., Zhang, Q., Zhang, Y., Jiang, X., and Fu, S. (2006) Lectin-conjugated PEG-PLA nanoparticles: Preparation and brain delivery after intranasal administration. *Biomaterials 27*, 3482–3490.

(16) Oishi, M., Kataoka, K., and Nagasaki, Y. (2006) pH-Rsponsive three-layered PEGylated polyplex micelle based on a lactosylated ABC triblock copolymer as a targetable and endsome-disruptive nonviral gene vector. *Bioconjugate Chem. 16*, 677–688.

(17) Bae, Y., Jang, W-D., Nishiyama, N., Fukushima, S., and Kataoka, K. (2005) Multifunctional polymeric micelles with folate-mediated cancer cell targeting and pH-triggered drug releasing properties for active intracellular drug delivery. *Mol. BioSyst. 1*, 242–250.

(18) Wu, P., Feldman, A. K., Nugent, A. K., Hawker, C. J., Scheel, A., Voit, B., Pyun, J., Frechet, J. M. J., Sharpless, K. B., and Fokin, V. V. (2004) Efficiency and fidelity in a click-chemistry route to triazole dendrimers by the copper(I)-catalyzed ligation of azides and alkynes. *Angew. Chem., Int. Ed. 43*, 3928–3932.

(19) Malkoch, M., Vestberg, R., Gupta, N., Mespouille, L., Dubois, Ph., Mason, A. F., Hedrick, J. L., Liao, Q., Frank, C. W., Kingsbury, K., and Hawker, C. J. (2006) Synthesis of well-defined hydrogel networks using Click chemistry. *Chem. Commun.* 2774–2776.

(20) Lutz, J. F. (2007) 1,3-Dipolar cycloadditions of azides and alkynes: A universal ligation tool in polymer and materials Science. *Angew. Chem., Int. Ed. 46*, 1018–1025.

(21) Rostovtsev, V. V., Green, L. G., Fokin, V. V., and Sharpless, K. B. (2002) A stepwise Huisgen cycloaddition process: Copper (I)-catalyzed regioselective ligation of azides and terminal alkynes. *Angew. Chem., Int. Ed. 41*, 2596–2599.

(22) Wang, Q., Chan, T. R., Hilgraf, R., Fokin, V. V., Sharpless, K. B., and Finn, M. G. (2003) Bioconjugation by Copper (I)-catalyzed azide-alkyne [3 + 2] cycloaddition. *J. Am. Chem. Soc. 125*, 3192–3193.

(23) Link, A. J., and Tirrell, D. A. (2003) Cell surface labeling of *Escherichia coli* via copper (I)-catalyzed [3 + 2] cycloaddition. *J. Am. Chem. Soc. 125*, 11164–11165.

(24) Deiters, A., Cropp, T. A., Mukherji, M., Chin, J. W., Anderson, J. C., and Schultz, P. G. (2003) Adding amino acids with novel reactivity to the genetic code of *Saccharomyces cerevisiae*. *J. Am. Chem. Soc. 125*, 11782–11783.

(25) Breitenkamp, K., Sill, K., and Skaff, H. Heterobifunctional poly(ethylene glycol), uses thereof and intermediates thereto. PCT Int. Appl. WO 2006047419, 2006

(26) Hassane, F. S., Frisch, B., and Schuber, F. (2006) Targeted liposomes: Convenient coupling of ligands to performed vesicles using "Click Chemistry". *Bioconjugate Chem. 17*, 849–854.

(27) Brennan, J. L., Hatzakis, N. S., Tshikhudo, T. R., Dirvianskyte, N., Razumas, V., Patkar, S., Vind, J., Svendsen, A., Nolte, R. J. M., Rowan, A. E., and Brust, M. (2006) Bionanoconjugation via click chemistry: The creation of functional hybrids of lipases and gold nanoparticles. *Bioconjugate Chem. 17*, 1373–1375.

(28) Fluka Catalogue, #17758. (11-Azido-3,6,9-trioxaundecan-1-amine), >90% (GC).

(29) Szwarc, M., Levy, M., and Milkovich, R. (1956) Polymerization initiated by electron transfer to monomer. A new method of formation of block polymers. *J. Am. Chem. Soc. 78*, 2656.

(30) Garanti, L., and Molteni, G. (2003) MeOPEG-bounded azide cycloadditions to alkynyl dipolarophiles. *Tetrahedron Lett. 44*, 1133–1135.

(31) Cammas, S., Nagasaki, Y., and Kataoka, K. (1995) Heterobifunctional poly(ethylene oxide): synthesis of α-methoxy-ω-amino and α-hydroxy-ω-amino PEOs with the same molecular weights. *Bioconjugate Chem. 6*, 226–230.

(32) Bertozzi, C. R., and Bednarski, M. D. (1991) The synthesis of heterobifunctional linkers for the conjugation of ligands to molecular probes. *J. Org. Chem. 56*, 4326–4329.

(33) Iyer, S. S., Anderson, A. S., Reed, S., Swanson, B., and Schmidt, J. G. (2004) Synthesis of orthogonal end functionalized oligoethylene glycols of defined lengths. *Tetrahedron Lett. 45*, 4285–4288.

(34) Zalipsky, S. (1995) Functionalized poly(ethylene glycol) for preparation of biologically relevant conjugates. *Bioconjugate Chem. 6*, 150–165.

(35) Smith, M. B., March, J., Eds. (2001) *March's Advanced Organic Chemistry. Reactions, Mechanisms, and Structure*, 5 th ed. p 1412, John Wiley & Sons, New York.

(36) McManus, S. P., Karaman, R. M., Sedaghat-Herati, M. R., Shannon, T. G., Hovatter, T. W., and Harris, J. M. (1990) Chain-cleavage and hydrolysis of activated polyethylene glycol derivatives: Evidence for competitive processes. *J. Polym. Sci., Part A: Polym. Chem. 28*, 3337–3346.

BC700152J

Available online at www.sciencedirect.com
ScienceDirect
Biomaterials 28 (2007) 5169–5175
Biomaterials
www.elsevier.com/locate/biomaterials

Gene delivery with biocompatible cationic polymer: Pharmacogenomic analysis on cell bioactivity

Kayo Masago[a,1], Keiji Itaka[a,1], Nobuhiro Nishiyama[a], Ung-il Chung[a,c,d], Kazunori Kataoka[a,b,d,*]

[a]*Division of Clinical Biotechnology, Center for Disease Biology and Integrative Medicine, Graduate School of Medicine, The University of Tokyo, Japan*
[b]*Department of Materials Science and Engineering, Graduate School of Engineering, The University of Tokyo, Japan*
[c]*Department of Bioengineering, Graduate School of Engineering, The University of Tokyo, Japan*
[d]*Center for Nanobio Integration, The University of Tokyo, 7-3-1 Hongo, Bunkyo-ku, Tokyo 113-0033, Japan*

Received 7 June 2007; accepted 10 July 2007
Available online 30 July 2007

Abstract

The availability of non-viral gene delivery systems is determined by their capacity and safety during gene introduction. In this study, the safety issues of polyplex were analyzed from the standpoint of the biomolecular mechanisms. P[Asp(DET)], a newly developed polymer, polyasparagine carrying the *N*-(2-aminoethyl)aminoethyl group as the side chain which was recently revealed to show good transfection efficiency to primary cells, was compared to conventional linear poly(ethylenimine) (LPEI). After transfection toward a bioluminescent cell line, P[Asp(DET)] maintained the expression level of stably expressing luciferase. In contrast, LPEI showed a decrease in the luciferase expression, while the similar expression of exogenous reporter gene was obtained. Evaluation of the housekeeping genes expression as well as the profiles of pDNA uptake after transfection suggested the time-dependent toxicity of LPEI that perturbs cellular homeostasis. Consistently, the induction of osteogenic differentiation by functional gene introduction was achieved only by P[Asp(DET)], even though appreciable expression of the gene was achieved by LPEI. It is crucial that this aspect of safety be taken into account, especially when the gene introduction is applied to primary cells to regulate such cell function as differentiation. This biomolecular analysis focusing on cellular homeostasis is beneficial for assessing the practicability of the gene delivery systems for clinical application.
© 2007 Elsevier Ltd. All rights reserved.

Keywords: Biocompatibility; Gene transfer; Cationic polymer; Cytotoxicity; Cell differentiation

1. Introduction

Gene therapies have attracted progressive attention for the treatment of numerous intractable diseases, but the lack of safe and efficient gene-delivery systems is an obstacle to their clinical application. Viral vectors are known to be highly potent gene delivery systems, yet may also induce adverse side effects, including severe immunological and toxicological responses. In fact, recent clinical trials using viral vectors have been halted due to unprecedented toxicity, including the death of a patient [1–4]. Therefore, non-viral gene carriers such as cationic lipids and polymers are expected to be an alternative to viral vectors directing therapeutic genes to target tissues.

The availability of gene carriers is largely determined by their transfection efficiency and cytotoxicity. Although the latter is generally evaluated through the viability assay of cultured cells such as an MTT assay [5], an MTT assay only reflects the non-specific outcome of cell death. Synthetic carriers may induce side effects including complement activation, carcinogenicity, teratogenicity and immunogenicity, all of which are serious concerns for clinical application [6]. Thus, the safety issues of non-viral gene carriers, both on a cellular and systemic basis,

*Corresponding author. Department of Materials Engineering, Graduate School of Engineering, The University of Tokyo, 7-3-1 Hongo, Bunkyo-ku, Tokyo 113-0033, Japan. Tel.: +81 3 5841 7138; fax: +81 3 5841 7139.
E-mail address: kataoka@bmw.t.u-tokyo.ac.jp (K. Kataoka).
[1]These authors contributed equally to this work.

0142-9612/$ - see front matter © 2007 Elsevier Ltd. All rights reserved.
doi:10.1016/j.biomaterials.2007.07.019

are critical for their clinical development, requiring careful analysis of the toxicity by exploring the biomolecular mechanisms. In this regard, a pharmacogenomic analysis of the global gene expression in the transfected cells is of particular interest. This approach has recently been advocated as polymer genomics or material genomics, and several studies have been reported to have applied it for the evaluation of non-viral gene carriers [7,8].

Recently, we developed a novel block catiomer-based gene delivery system that showed excellent capacity for *in vitro* transfection to primary cells [9]. This system is composed of plasmid DNA (pDNA) and poly(ethyleneglycol)-block-polyasparagine carrying the *N*-(2-aminoethyl) aminoethyl group $(CH_2)_2NH(CH_2)_2NH_2$ as the side chain (PEG-PAsp[DET]). Ethylene diamine units located at the side chain are only half protonated under neutral pH and are thus feasible candidates to perform the so-called proton sponge effect, which has been believed to be the major mechanism for the excellent transfection efficiency of some polyamine derivatives having substantially lowered pKa such as poly(ethylenimine) (PEI) [10–12]. As well as the good transfection efficiency, the polyplex micelles from this block catiomer showed minimal cytotoxicity toward various primary cells, achieving the successful *in vivo* gene introduction to the vascular lesions [13] and the effective induction of cell differentiation both *in vitro* and *in vivo* through the effective expression of the genes encoding transcriptional factors [14].

These results motivated us to perform an additional toxicogenomic study of P[Asp(DET)] in order to ensure the safety for future clinical application. Linear PEI (LPEI) was used as a control, representing the common polycation for the construction of polyplexes. Although P[Asp(DET)] and LPEI both have a buffering capacity under an endosomal pH, they showed a considerable difference in the toxicological profiles which revealed the appreciably lowered toxicity of the former compared to the latter. In particular, the time-dependent change in the pharmacogenomical toxicity toward the targeted cells was evaluated in detail, in regards to the capacity of inducing cell differentiation through the transfection of functional genes encoded in the encapsulated pDNA in the polyplex.

2. Materials and methods

2.1. Materials

pGL3-control pDNA encoding firefly luciferase (Promega, Madison, WI, USA), pRL-CMV pDNA encoding renilla luciferase (RL) (Promega), and EGFP-C1 pDNA encoding EGFP (Clontech, Palo Alto, CA, USA) were amplified in the *Escherichia coli* strain DH5α, which was isolated and purified using a QIAGEN HiSpeed Plasmid Maxi Kit (Qiagen, Hilden, Germany). pCMV5 pDNA expressing HA-tagged mouse caALK6 and pcDEF3 pDNA expressing Flag-tagged mouse Runx2 were generous gifts from Dr. M. Krüppel (Mt. Sinai Hospital, Toronto, ON, Canada) and Dr. K. Miyazono (University of Tokyo, Tokyo, Japan), respectively. The concentration of DNA was determined by measuring the UV absorption at 260 nm.

2.2. Cells

HuH-7 cells were obtained from the Riken Cell Bank (Tsukuba, Japan). Bioluminescent cells (HuH-7-luc) stably expressing firefly luciferase were kindly provided by Mr. S. Matsumoto (University of Tokyo). Dulbecco's modified Eagle's medium (DMEM) and fetal bovine serum (FBS) were purchased from Sigma-Aldrich (St. Louis, MO, USA).

2.3. Polycations for the preparation of polyplex

LPEI (Exgen 500, $M_w = 22$ kDa) was purchased from MBI Fermentas (Burlington, ON, Canada). Diethylenetriamine (DET) was purchased from Tokyo Kasei Kogyo (Tokyo, Japan). All other chemicals were purchased from Wako Pure Chemical Industries (Osaka, Japan). P[Asp(DET)] was synthesized by the side-chain aminolysis reaction of the poly (β-benzyl L-aspartate) (PBLA) as previously reported [9]. Briefly, the PBLA was synthesized by the ring-opening polymerization of the β-benzyl-L-aspartate *N*-carboxyanhydride (BLA-NCA) initiated by the primary amine of *n*-butylamine in *N*,*N*-dimethylformamide (DMF)/dichloromethane (1:10) at 40 °C, followed by the acetylation of the *N*-terminal amine with acetic anhydride. Gel permeation chromatography (GPC) was performed to confirm a unimodal molecular weight distribution (M_w/M_n 1.20) of PBLA by TOSHO HLC-8220 (columns: TSK-gel G4000HHR + G3000HHR, eluent: DMF + 10 mM LiCl, $T = 40$ °C, detector: refractive index). The degree of polymerization of PBLA was determined as 98 from the ^{1}H NMR spectrum (JEOL EX300 spectrometer: JEOL, Tokyo, Japan). Then, the side-chain aminolysis reaction of PBLA was performed by mixing the DMF solution of PBLA(50 mg/ml) with a 50-fold excess of DET in DMF at 40 °C to obtain P[Asp(DET)].

2.4. Polyplex formation

Each polyplex sample with a pDNA concentration of 33 μg/mL was prepared by simply mixing pDNA and polycation(LPEI or P[Asp(DET)]) at the indicated *N*/*P* ratio (= [total amines in polycation]/[DNA phosphates]) in a 10 mM Tris–HCl (pH 7.4) buffer solution.

2.5. Dual luciferase measurement on HuH-7-luc cells transfected with pRL-CMV pDNA

HuH-7-luc cells were seeded on 96-well culture plates (3×10^3 cells/well) and incubated overnight in 100 μl DMEM supplemented with 10% FBS and penicillin/streptomycin. After the culture medium was replaced with fresh medium containing 10% FBS, 5.5 μl of the polyplexes composed of P[Asp(DET)] or LPEI (final DNA concentration: 33 μg/ml) were applied to each well. After 24 h, the medium was changed to remove the polyplexes, followed by further incubation for 24 or 48 h. The firefly and RL activities were measured using a Dual-Luciferase Reporter Assay System (Promega) according to the protocol provided by the manufacturer, using a GloMax™ 96 Microplate Luminometer (Promega).

2.6. Cell proliferation assay

HuH-7-luc cells (6×10^4 cells/well) were seeded in six-well plates and cultured overnight. After the transfection as described above (polyplex solution: 90 μl/well), the cells were washed with phosphate-buffered saline (PBS), trypsinized, and scraped off. Then the cell number was counted by a nucleo counter (Chemometec, Tokyo, JAPAN) following the protocol provided by the manufacturer. The measurement was duplicated.

2.7. Lactate dehydrogenase (LDH) assay

The degree of membrane destabilization was examined by lactate dehydrogenase (LDH) activity liberated from the cytoplasm. The cells were plated on 96-well plates and incubated overnight in 100 μl of DMEM

containing 10% FBS. Then the medium was changed and 5.5 μl of polyplex was added to each well similarly as in the transfection described above. After 4, 8, or 24 h, the plates were centrifuged for 5 min at 110*g*. Then, 50 μl of aliquots in each well were collected and subjected to the LDH measurement. A CytoTox 96 Non-Radioactive Cytotoxicity Assay kit (Promega) was used following the protocol provided by the manufacturer, using a plate reader AD200 (Beckman Coulter, Inc., USA) for reading the OD at 490 nm to determine the amount of the produced diformazan. Freeze-chaw cells were used to calibrate 100% LDH activity. To compare the cytotoxicity between P[Asp(DET)] and LPEI, the parametrical analysis using the Student's *t*-test was performed.

2.8. Quantitative assay on the cellular uptake of pDNA by real-time quantitative PCR

EGFP-C1 pDNA expressing EGFP was transfected to HuH-7. 8×10^4 HuH-7 cells/well were plated in six-well plates and cultured overnight, and then the transfection was done similarly as described before. At the indicated time periods (4, 8 and 24 h), the DNA was collected and purified from each well using a Wizard Genomic DNA purification Kit (Promega), then subjected to the PCR for the quantification of pDNA copies encoding EGFP. The copy number of β-actin (βA) was also determined by the ABI 7500 Fast Real-Time PCR systems to normalize the cell number (Applied Biosystems, Foster City, CA, USA). The sequences of the primers and probe used for EGFP were as follows: forward primer GGGCACAAGCTGGAGTACAAC and reverse primer TCTGCTT GTCGGCCATGATA. The sequence of the probe was ACAGCCA CAACGTCT with FAM as a fluorescent dye on the 5-end and MGB as a fluorescence quencher dye labeled on the 3-end. For βA amplification and quantitation, the forward and reverse primers and probe were purchased as a standard TaqMan gene expression assay kit from Applied Biosystems. PCR was done for 20 s at 95 °C, followed by 3 s at 95 °C and 60 s at 60 °C for 40 cycles. A linear relationship between the number of cells and threshold cycle for the βA gene amplification was confirmed (data not shown).

2.9. Evaluation of osteocalcin mRNA expression

Osteogenic differentiation of the mouse calvarial cells was evaluated by the expression of osteocalcin mRNA, an osteoblast-differentiation marker. Mouse calvarial cells were isolated from the calvariae of neonatal littermates. The experimental procedures were handled in accordance with the guidelines of the Animal Committee of the University of Tokyo. Calvariae were digested for 10 min at 37–8 °C in an enzyme solution containing 0.1% collagenase and 0.2% dispase for five cycles. Cells isolated by the final four digestions were combined and cultured in DMEM supplemented with 10% FBS and penicillin/streptomycin. For induction of the differentiation assays, 3×10^4 primary mouse calvarial cells were plated in six-well culture plates and cultured for 24 h. After changing the medium to that containing 10% FBS and dexamethazone, polyplexes containing pDNAs expressing caALK6 and Runx2 were applied to each well by a similar transfection procedure as that previously described. The culture medium was refreshed on Day 3 after transfection, then changed every 3 days. On Days 5 and 11, the cells were washed with PBS and the total RNA was collected using the RNeasy Mini Preparation Kit (Qiagen) according to the manufacturer's protocol. Gene expression was analyzed by a quantitative PCR. 500 ng of total RNA was analyzed in a final volume of 50 μl. Reverse transcription was performed for 30 min at 50 °C followed by PCR: 50 °C for 2 min, 95 °C for 10 min, followed by 40 cycles of 95 °C for 15 s and 60 °C for 1 min using the Quantitect SYBR Green PCR Kit (Qiagen). Each mRNA expression was normalized to levels of mouse βA mRNA. The primers used were as follows: osteocalcin: forward primer (AAGCAGGAGGGCAATAAGGT) and reverse primer (TTTGTAGGCGGTCTTCAAGC); mouse βA: forward primer (AGATGTGGATCAGCAAGCAG), reverse primer (GCGCAAGT-TAGGTTTTGTCA). To compare the osteocalcin expressions using P[Asp(DET)] or LPEI, the parametrical analysis using the Student's *t*-test was performed.

2.10. Housekeeping gene expression assay

After a similar transfection procedure as previously described was performed, the total RNA was collected at 24 or 72 h. To evaluate the expressions of the housekeeping genes, a Taqman Human Endogenous Control Plate (Applied Biosystems) was used according to the manufacturer's protocol, including 18S rRNA, acidic ribosomal protein (PO), βA, cyclophilin (CYC), glyceraldehyde-3-phosphate dehydrogenase (GAPDH), phosphoglycero-kinase (PGK), β2-microglobulin (β2m), β-glucronidase (GUS), hypoxanthine ribosyl transferase (HPRT), TATA binding protein (TBP) and transferrin receptor (TfR). The control cells serve as a baseline for the assays and are shown as zero on the graph. The results are expressed in the comparative cycle threshold; ΔC_T, greater than or less than the control ΔC_T.

3. Results and discussion

3.1. In vitro transfection toward bioluminescent cell line

The bioluminescent human hepatoma cell line (HuH-7-Luc) stably expressing firefly luciferase (Luc) was used to evaluate the pharmacogenomic influence as well as the transfection efficiency of the polyplexes. After the transfection of RL using P[Asp(DET)] or LPEI, both the Luc and RL expressions were estimated simultaneously. The expressions were normalized by the number of cells, which were directly counted after scraping the cells from the culture plates.

The exogenous RL expressions per cell in Fig. 1(a) showed that the P[Asp(DET)] polyplex had comparable transfection efficiency to the LPEI polyplex giving the highest expression at 48 h after transfection. In contrast, the endogenous Luc expression showed a different profile between the two polyplexes; the Luc expression of the cells transfected by the P[Asp(DET)] polyplex was equivalent as that of the control cells, while the cells transfected by the LPEI polyplex showed a gradual decrease in Luc expression per cell (Fig. 1(b)). The cell numbers shown in Fig. 1(c) revealed that the proliferation was significantly inhibited by the transfection using LPEI after Day 2, compared to that of the other two groups (the cells transfected by P[Asp(DET)] and the control). Note that in these experiments, the polyplexes in the medium were removed at 24 h after transfection by changing the culture medium. Thus, these results suggest that although the exogenous RL gene expression showed an increase until Day 2, the internalized LPEI into the target cells by Day 1 had some continuous inhibiting effects on the proliferation and endogenous gene expression in the targeted cells. It is reasonable to assume that the LPEI released from the polyplex may impair the intracellular activities in a time-dependent manner.

3.2. Investigation of the cytotoxicity induced by LPEI

To investigate the detailed mechanisms of the time-dependent cytotoxicity possibly induced by LPEI, we

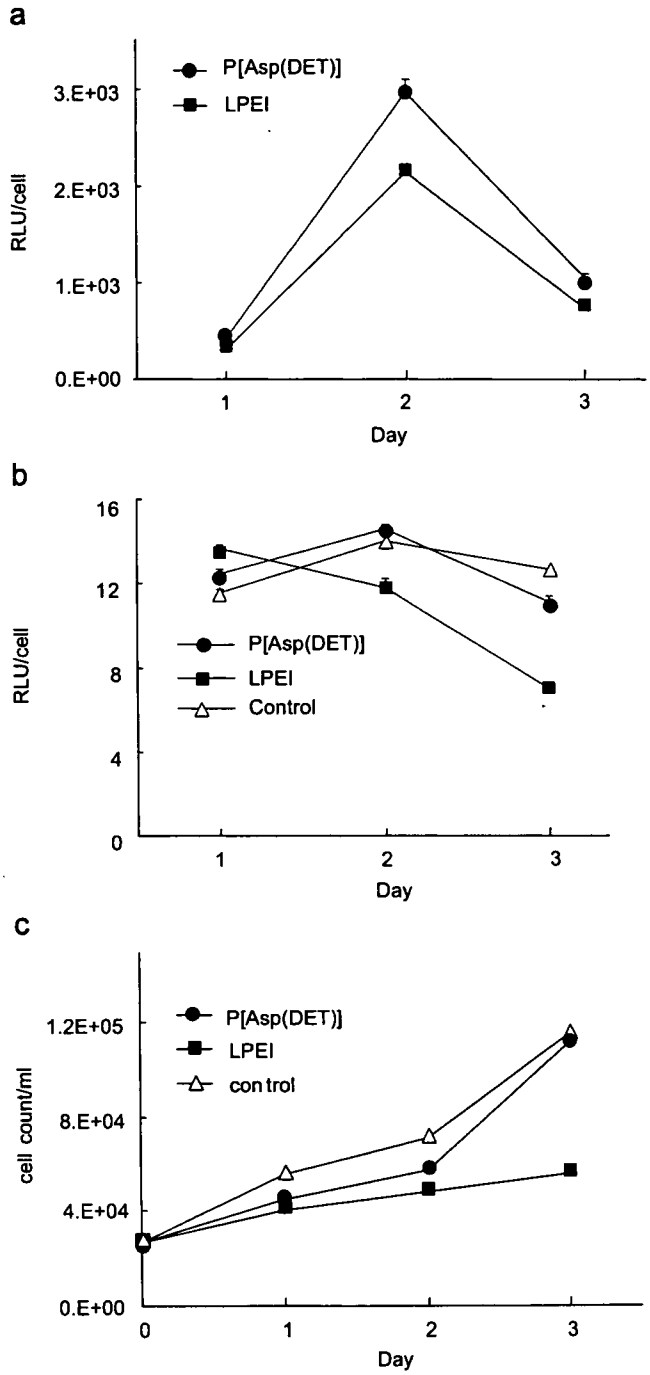

Fig. 1. *In vitro* transfection toward HuH-7-Luc cells. (a) Exogenous renilla luciferase expression. (b) Endogenous firefly luciferase expression. (c) Cell proliferation assay. Transfection was performed by P[Asp(DET)] (closed circle) or LPEI (closed square) polyplexes formed at $N/P = 10$. Gene expression was evaluated for 3 days after transfection and normalized by the cell number. Each data of gene expression represents mean ± SD ($n = 8$). The data of cell number are means ($n = 2$).

further assessed each step involved in the transfection process. The first step is apparently the cellular association and internalization of the gene carriers. It is assumed that these events may evoke membrane destabilization, possibly

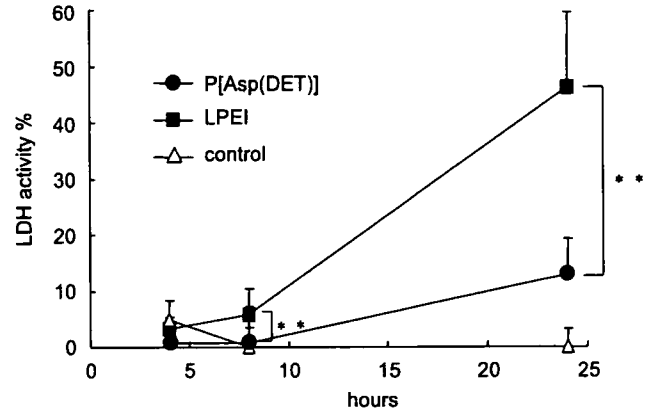

Fig. 2. Evaluation of LDH activity after transfecton using P[Asp(DET)] (closed circle) or LPEI (closed square) polyplexes. Each data represents mean ± SD ($n = 8$). Freeze-chaw cells were used to calibrate 100% LDH activity. $^{**}P<0.01$.

causing cytotoxic effects [15]. The change in membrane permeability due to the interaction with the polyplexes was examined by an LDH assay under the same condition as used in the transfection experiments above. As presented in Fig. 2, the cells transfected by the LPEI polyplex revealed a time-dependent increase in the leakage of LDH until 24 h after transfection. In contrast, the P[Asp(DET)] polyplex induced a minimal LDH leakage compared to the control. Considering the similar cationic nature of LPEI and P[Asp(DET)], the membrane destabilization after their association onto the plasma membrane is expected to be similar, which is apparently not the case observed here. The discrepancy between the two polymers on the time-dependent LDH leakage suggests that factors other than simple electrostatic interaction play a substantial role in the process of membrane destabilization.

The uptake amount of reporter gene into the HuH-7 cells by the P[Asp(DET)] or LPEI polyplex was determined by a real-time PCR in terms of gene copies per cell from the total DNA samples [16–18]. As seen in Fig. 3(a), the uptake amount of reporter gene showed a continuous increase until 24 h after the transfection in the case of the P[Asp(DET)] polyplex. The amount of reporter genes internalized with the LPEI polyplex was similar to that with the P[Asp(DET)] polyplex at 8 h, yet was significantly reduced by extending the transfection time to 24 h. One possible reason for this phenomenon might be the rapid dissociation of pDNA from LPEI in the cytoplasm as reported in the literature [19], resulting in its fast degradation by cytoplasmic enzymes [20,21]. However, when the culture medium was changed to remove the polyplexes at 4 h after the transfection, both systems showed a similar profile of a gradual decrease in the copy number after the medium change (Fig. 3(b)), suggesting the similar stability of the internalized pDNAs for both systems. These results suggest that the decrease in the internalized amount of the reporter gene with the LPEI polyplex shown in Fig. 3(a) may be due to

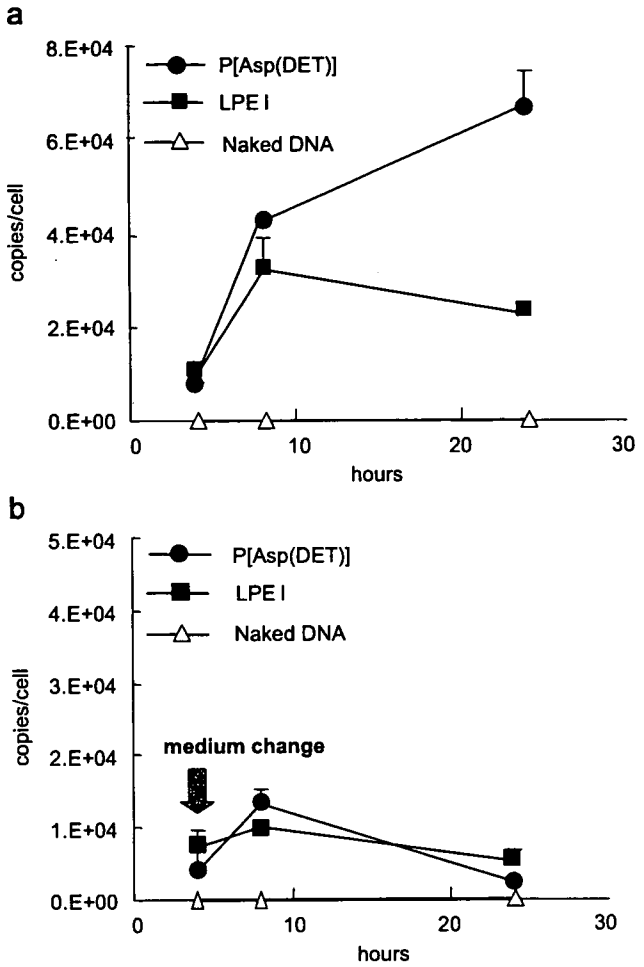

Fig. 3. Evaluation of pDNA uptake after transfecton using P[Asp(DET)] (closed circle), LPEI (closed square), or by the form of naked pDNA (open triangle). The cellular uptake of pDNA was quantified by a PCR, (a) without changing medium during the procedure, or (b) with medium change after 4 h of transfection. Each data represents mean ± SD ($n = 3$).

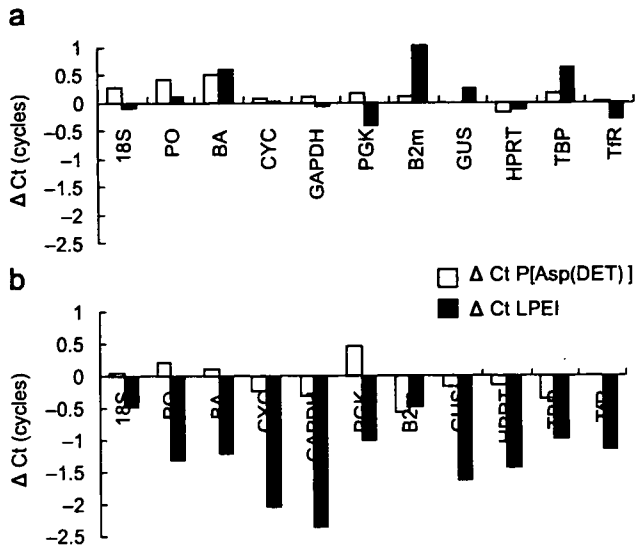

Fig. 4. Housekeeping genes expression after transfection. The mRNA expressions of various housekeeping genes were evaluated by a quantitative PCR at (a) 24 h and (b) 72 h after transfection using P[Asp(DET)] (open bar) or LPEI (filled bar).

the time-dependent decrease in the cellular activity to take up the polyplexes caused by the toxicity of LPEI.

To clarify this possible time-dependent influence on the cellular function from the viewpoint of the genomics, we assessed the change in the gene expressions of 11 frequently used housekeeping genes in the presence of the polyplex. These genes usually revealed a uniform expression, but the expression profile may vary in response to various external factors such as stress on the cells [22,23]. Thus, the variation in their expression profile is a good indicator for assessing the cellular function, a possible perturbation in the cellular homeostasis. The quantitative evaluation of the expression of these housekeeping genes by a real-time PCR revealed that the cells transfected by LPEI apparently showed downregulation in the expression of the housekeeping genes at 72 h after the transfection (Fig. 4(b)). Although the measurement at 24 h showed minimal fluctuation in the housekeeping gene expression, GAPDH and CYC were significantly downregulated by more than two cycles of ΔC_T values compared to those of the control cells at 72 h, indicating a four-fold decrease in gene expression. In these assays, the culture medium was changed at 24 h. Thus, it is likely that LPEI associated with the cells may induce the perturbed gene expression through the continuous interaction with intracellular components even after the medium change at 24 h to remove excess polyplexes in the medium. In contrast, the expression of these genes in the cells transfected by P[Asp(DET)] retained constant even after 72 h, all of which were within 0.5 cycles compared to those of the control cells. These results of the housekeeping gene expressions suggest the sustained homeostasis through the transfection process using P[Asp(DET)], leading to constant cellular activity such as the polyplex uptake (Fig. 3(a)), proliferation (Fig. 1(c)), and continuous gene expression (Fig. 1(b)).

As was occasionally reported, polyplexes induce critical cytotoxicity especially at higher N/P ratios, presumably due to the presence of free polymers [24–26]. Although the mechanisms are likely to involve various cellular responses such as immunostimulation [27] and apoptosis [15,28], the plasma membrane perturbation associated with the cationic polymers may be an initial event that induces the toxicity [28,29]. From our present results on LDH release (Fig. 2), the disorder on the plasma membrane seems to occur within 24 h after the transfection with the LPEI polyplex. In addition, the intracellular events that were noticed as the change in the endogenous gene expressions emerged after 72 h of transfection. It should be noted that these events of the perturbed expression of endogenous genes were inevitable even after further supply of the polyplexes was halted by the medium change at 24 h, strongly suggesting that the free PEI remaining inside the

cells after the polyplex dissociation may cause an unfavorable interaction with the intracellular components in a time-dependent manner.

3.3. Transfection toward mouse calvarial cells and induction of osteogenic differentiation

The data so far indicates the minimal cytotoxicity of P[Asp(DET)], suggesting a feasible capacity in gene delivery for therapeutic purposes. To assess this feasibility, we evaluated the induction of cell differentiation by exogenous gene introduction. pDNAs encoding bioactive factors, caALK6 and Runx2, both of which were revealed to induce the effective osteogenic differentiation [30], were introduced in this way to mouse calvarial cells derived from neonatal calvariae. The osteogenic differentiation was evaluated by the expression of osteocalcin mRNA, a specific osteoblast-differentiation marker. As shown in Fig. 5, the time-dependent increase in osteocalcin expression was confirmed after the transfection of caALK6+Runx2 using P[Asp(DET)]. In contrast, no sign of the osteocalcin expression was observed by the LPEI polyplex until Day 11. Notably, the GFP-encoding pDNA, a negative control of differentiation, achieved almost identical GFP expression by the P[Asp(DET)] and LPEI polyplexes, without apparent morphologic changes in the targeted cells as observed under the microscope (data not shown). It can be reasonably assumed that, with the same transfection procedure, the osteogenic factors of caALK6 and Runx2 were also expressed similarly inside the targeted cells by the P[Asp(DET)] and LPEI polyplexes. Therefore, the lack of osteocalcin induction by the LPEI polyplex is considered to be due to the adverse effect on cell bioactivity by LPEI. In contrast, P[Asp(DET)] was revealed to be available for practical use in the induction of cell differentiation.

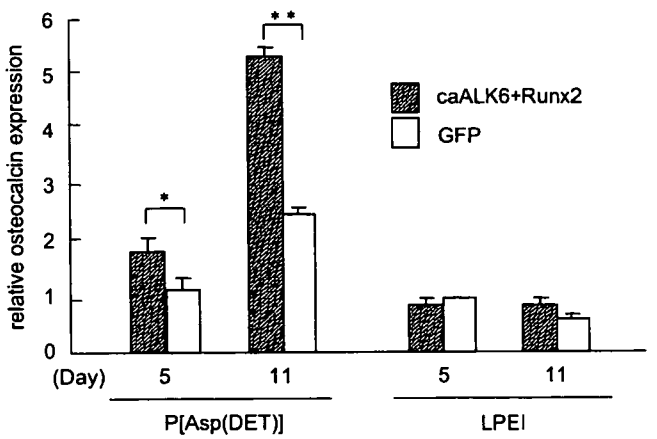

Fig. 5. Evaluation of osteocalcin mRNA expression by a quantitative PCR. Osteogenic differentiation was induced on the mouse calvarial cells by transfection of caALK6 and Runx2 (hatched bar) using P[Asp(DET)] or LPEI. As a negative control, a GFP (open bar) gene was used. After 5 or 11 days of transfection, the total RNA was collected and the osteocalcin expression was estimated. Each data represents mean±SD ($n = 3$). $^{*}P<0.05$ and $^{**}P<0.01$.

4. Conclusions

In conclusion, although LPEI has been widely used for gene introduction to various cell lines, the time-dependent cytotoxicity, which perturbs cellular homeostasis, should be carefully considered even though an appreciable expression of the reporter gene was achieved. As exemplified here in the osteogenic differentiation, impaired cellular function gave a negative effect in the intracellular signal transduction directing cell differentiation. This aspect of toxicity should be carefully counted especially when gene therapy is proposed to promote such cell functions as differentiation. Worth noting in this regard is the excellent capacity of the gene introduction of P[Asp(DET)] with minimal toxic effects, indicating that this system holds much promise for the therapeutic applications of gene therapy requiring safe and regulated gene expressions.

Acknowledgments

We thank Dr. M. Krüppel and Dr. K. Miyazono for pDNAs expressing caALK6 and Runx2, respectively. This work was supported by Grants-in-Aid for Scientific Research from the Japanese Ministry of Education, Culture, Sports, Science and Technology (#15390452 and #17390412), Health Science Research Grants from the Japanese Ministry of Health, Labor and Welfare (#H17-Immunology-009), and the Core Research Program for Evolutional Science and Technology (CREST) from the Japan Science and Technology (JST) Agency.

References

[1] Marshall E. Gene therapy death prompts review of adenovirus vector. Science 1999;286(5448):2244–5.
[2] Hollon T. Researchers and regulators reflect on first gene therapy death. Nat Med 2000;6(1):6.
[3] Assessment of adenoviral vector safety and toxicity: report of the National Institutes of Health Recombinant DNA advisory committee. Hum Gene Ther 2002;13(1):3–13.
[4] Gansbacher B. Report of a second serious adverse event in a clinical trial of gene therapy for X-linked severe combined immune deficiency (X-SCID). Position of the European Society of Gene Therapy (ESGT). J Gene Med 2003;5(3):261–2.
[5] Mosmann T. Rapid colorimetric assay for cellular growth and survival: application to proliferation and cytotoxicity assays. J Immunol Methods 1983;65(1–2):55–63.
[6] Duncan R. The dawning era of polymer therapeutics. Nat Rev Drug Discov 2003;2(5):347–60.
[7] Omidi Y, Hollins AJ, Benboubetra M, Drayton R, Benter IF, Akhtar S. Toxicogenomics of non-viral vectors for gene therapy: a microarray study of lipofectin- and oligofectamine-induced gene expression changes in human epithelial cells. J Drug Target 2003;11(6):311–23.
[8] Kabanov AV, Batrakova EV, Sriadibhatla S, Yang Z, Kelly DL, Alakov VY. Polymer genomics: shifting the gene and drug delivery paradigms. J Control Release 2005;101(1-3):259–71.

[9] Kanayama N, Fukushima S, Nishiyama N, Itaka K, Jang WD, Miyata K, et al. A PEG-based biocompatible block catiomer with high buffering capacity for the construction of polyplex micelles showing efficient gene transfer toward primary cells. Chem Med Chem 2006;1(4):439–44.
[10] Boussif O, Lezoualc'h F, Zanta MA, Mergny MD, Scherman D, Demeneix B, et al. A versatile vector for gene and oligonucleotide transfer into cells in culture and in vivo: polyethylenimine. Proc Natl Acad Sci USA 1995;92(16):7297–301.
[11] Boletta A, Benigni A, Lutz J, Remuzzi G, Soria MR, Monaco L. Nonviral gene delivery to the rat kidney with polyethylenimine. Hum Gene Ther 1997;8(10):1243–51.
[12] Goula D, Benoist C, Mantero S, Merlo G, Levi G, Demeneix BA. Polyethylenimine-based intravenous delivery of transgenes to mouse lung. Gene Ther 1998;5(9):1291–5.
[13] Akagi D, Oba M, Koyama H, Nishiyama N, Fukushima S, Miyata T, et al. Biocompatible micellar nanovectors achieve efficient gene transfer to vascular lesions without cytotoxicity and thrombus formation. Gene Ther 2007;14(13):1029–38.
[14] Itaka K, Ohba S, Chung U, Kataoka K. Bone regeneration by regulated in vivo gene transfer using biocompatible polyplex nanomicelles. Mol Ther 2007; Epub ahead of print.
[15] Moghimi SM, Symonds P, Murray JC, Hunter AC, Debska G, Szewczyk A. A two-stage poly(ethylenimine)-mediated cytotoxicity: implications for gene transfer/therapy. Mol Ther 2005;11(6):990–5.
[16] Lehmann MJ, Sczakiel G. Spontaneous uptake of biologically active recombinant DNA by mammalian cells via a selected DNA segment. Gene Ther 2005;12(5):446–51.
[17] Varga CM, Tedford NC, Thomas M, Klibanov AM, Griffith LG, Lauffenburger DA. Quantitative comparison of polyethylenimine formulations and adenoviral vectors in terms of intracellular gene delivery processes. Gene Ther 2005;12(13):1023–32.
[18] Hama S, Akita H, Ito R, Mizuguchi H, Hayakawa T, Harashima H. Quantitative comparison of intracellular trafficking and nuclear transcription between adenoviral and lipoplex systems. Mol Ther 2006;13(4):786–94.
[19] Itaka K, Harada A, Yamasaki Y, Nakamura K, Kawaguchi H, Kataoka K. In situ single cell observation by fluorescence resonance energy transfer reveals fast intra-cytoplasmic delivery and easy release of plasmid DNA complexed with linear polyethylenimine. J Gene Med 2004;6(1):76–84.
[20] Goncalves C, Pichon C, Guerin B, Midoux P. Intracellular processing and stability of DNA complexed with histidylated polylysine conjugates. J Gene Med 2002;4(3):271–81.
[21] Lechardeur D, Sohn KJ, Haardt M, Joshi PB, Monck M, Graham RW, et al. Metabolic instability of plasmid DNA in the cytosol: a potential barrier to gene transfer. Gene Ther 1999;6(4): 482–97.
[22] Thellin O, Zorzi W, Lakaye B, De Borman B, Coumans B, Hennen G, et al. Housekeeping genes as internal standards: use and limits. J Biotechnol 1999;75(2-3):291–5.
[23] Jain M, Nijhawan A, Tyagi AK, Khurana JP. Validation of housekeeping genes as internal control for studying gene expression in rice by quantitative real-time PCR. Biochem Biophys Res Commun 2006;345(2):646–51.
[24] Godbey WT, Wu KK, Mikos AG. Poly(ethylenimine)-mediated gene delivery affects endothelial cell function and viability. Biomaterials 2001;22(5):471–80.
[25] Morimoto K, Nishikawa M, Kawakami S, Nakano T, Hattori Y, Fumoto S, et al. Molecular weight-dependent gene transfection activity of unmodified and galactosylated polyethyleneimine on hepatoma cells and mouse liver. Mol Ther 2003;7(2):254–61.
[26] Boeckle S, von Gersdorff K, van der Piepen S, Culmsee C, Wagner E, Ogris M. Purification of polyethylenimine polyplexes highlights the role of free polycations in gene transfer. J Gene Med 2004; 6(10):1102–11.
[27] Regnstrom K, Ragnarsson EG, Koping-Hoggard M, Torstensson E, Nyblom H, Artursson P. PEI-a potent, but not harmless, mucosal immuno-stimulator of mixed T-helper cell response and FasL-mediated cell death in mice. Gene Ther 2003;10(18): 1575–83.
[28] Florea BI, Meaney C, Junginger HE, Borchard G. Transfection efficiency and toxicity of polyethylenimine in differentiated Calu-3 and nondifferentiated COS-1 cell cultures. AAPS PharmSci 2002;4(3):E12.
[29] Hunter AC. Molecular hurdles in polyfectin design and mechanistic background to polycation induced cytotoxicity. Adv Drug Deliv Rev 2006;58(14):1523–31.
[30] Ohba S, Ikeda T, Kugimiya F, Yano F, Lichtler A, Nakamura K, et al. Identification of a potent combination of osteogenic genes for bone regeneration using embryonic stem (ES) cell-based sensor. FASEBj 2007;21(8):1777–87.

Self-Assembled Nano-Bioreactor from Block Ionomers with Elevated and Stabilized Enzymatic Function

Akifumi Kawamura,[†] Atsushi Harada,*[,†] Kenji Kono,[†] and Kazunori Kataoka*[,‡,§]

Department of Applied Chemistry, Graduate School of Engineering, Osaka Prefecture University, 1-1 Gakuen-cho, Naka-ku, Sakai, Osaka 599-8531, Japan, Department of Materials Engineering, Graduate School of Engineering, and Center for NanoBio Integration, The University of Tokyo, 7-3-1 Hongo, Bunkyo-ku, Tokyo 113-8656, Japan. Received January 24, 2007; Revised Manuscript Received July 7, 2007

Core-cross-linked polyion complex (PIC) micelles entrapping trypsin in the core were prepared by mixing trypsin and poly(ethylene glycol)-*block*-poly(α,β-aspartic acid) in aqueous medium, followed by the introduction of glutaraldehyde cross-linkages. Trypsin incorporated into the core-cross-linked micelles showed high storage stabilities, and the initial enzymatic activity of trypsin was maintained even after standing for one week at ambient temperature. Further, stable compartmentalization of trypsin into the core-cross-linked micelles led to a unique modulation in the enzymatic functions including an improved thermal tolerability with an increased maximum reaction rate compared to native trypsin.

INTRODUCTION

Immobilized enzymes have been utilized in numerous applications including bioreactors, biosensors, and therapeutics (*1*–*5*). The major advantage of immobilized enzymes is an improvement in the storage and operational stabilities, which is especially crucial for proteolytic enzymes showing autolysis reaction. Conventionally, solid and porous matrices, including agarose, cellulose, and silica, have been used to immobilize enzymes through physical adsorption or covalent attachment. Also, water-soluble conjugates of enzymes with various polymers have been prepared (*6*–*9*). A novel approach to the immobilization of enzymes at the nanometric scale is the supramolecular assembly of nanoreactors. Noteworthy in this regard is the core–shell-type polyion complex (PIC) micelles formed from block ionomers. Charged enzymes can be incorporated into PIC micelles driven by electrostatic interaction in aqueous medium (*10*–*13*). Indeed, egg white lysozyme with cationic character was successfully incorporated into the core of PIC micelles through complexation with poly(ethylene glycol)-*block*-poly(α,β-aspartic acid) (PEG-PAA). Lysozyme-incorporated PIC micelles showed unique features including the on–off switching of an elevated enzymatic reaction synchronized with an external electric field. However, in the case of entrapping proteolytic enzymes (e.g., trypsin) in the micelles, autolysis was facilitated due to an increase in the local concentration of the enzyme. This problem has been recently overcome by the introduction of cross-linking into the core of PIC micelles (*14*). The tolerability of trypsin in PIC micelles, which is a typical proteolytic enzyme that selectively cleaves the bond adjacent to Lys and Arg, was dramatically improved by introducing cross-linking in the core of the micelles. Glutaraldehyde was used as a cross-linking reagent of the PIC micelles prepared by mixing trypsin and PEG-PAA. The core-cross-linked PIC micelles had a hydrogel core of nanoscopic size, formed by the cross-linking of trypsin and PAA, and an outer PEG shell layer. The core-cross-linked micelles might provide unique features in the field of nanoscopic enzymatic reactions.

Here, we studied in detail the enzymatic function of the core-cross-linked PIC micelles entrapping trypsin. Note that the Schiff base linkages in the cross-linked PIC micelles may undergo reductive amination to form alkylamine linkages. The amidase activity of entrapped trypsin in the micelle was evaluated by colorimetric assays using L-lysine *p*-nitroanilide as a substrate, both before and after the reductive amination. A remarkable improvement in the storing stability of trypsin was observed as a result of the compartmentalization of the enzyme into the cross-linked core of the PIC micelles. Further, an appreciable increase in the optimal temperature as well as a significantly improved tolerance to urea in the enzymatic reaction were achieved in the cross-linked micelles.

EXPERIMENTAL PROCEDURES

Materials. Poly(ethylene glycol)-poly(α,β-aspartic acid) block copolymer [PEG-PAA; 12 000 g/mol of PEG Mw; 68 of polymerization degree in PAA segment] was synthesized as described previously (*10*). Bovine pancreas trypsin, L-lysine *p*-nitroanilide and 3-methyl-2-benzothiazolinone hydrazone were purchased from Sigma (St. Louis, MO) and used without further purification. Sodium cyanotrihydroborate ($NaBH_3CN$), $Na_2HPO_4 \cdot 12H_2O$, $NaH_2PO_4 \cdot 2H_2O$, and 70% glutaraldehyde were reagent grade and were purchased from Wako Pure Chemical Industries (Osaka, Japan).

Preparation of Core-Cross-Linked PIC Micelles Entrapping Trypsin in the Core. Given amounts of trypsin and PEG-PAA were separately dissolved in sodium phosphate buffer (10 mM; pH 7.4) at 4 °C. The solutions were mixed at the optimum mixing ratio for PIC micelle formation, i.e., the ratio of the number of Asp residues in PEG-PAA against the total number of Lys and Arg residues in trypsin to be 0.75. The mixed

* To whom corresponding should be addressed. Prof. Kazunori Kataoka, Department of Materials Engineering, Graduate School of Engineering, The University of Tokyo, 7-3-1 Hongo, Bunkyo-ku Tokyo 113-8656, Japan, Tel: +81-3-5841-7138, Fax: +81-3-5841-7139, e-mail: kataoka@bmw.t.u-tokyo.ac.jp. Dr. Atsushi Harada, Department of Applied Chemistry, Graduate School of Engineering, Osaka Prefecture University, 1-1 Gakuen-cho, Naka-ku, Sakai, Osaka 599-8531, Japan, Tel & Fax: +81-72-254-9328, e-mail: harada@chem.osakafu-u.ac.jp.

† Osaka Prefecture University.

‡ Graduate School of Engineering, The University of Tokyo.

§ Center for NanoBio Integration, The University of Tokyo.

10.1021/bc070029t CCC: $37.00 © 2007 American Chemical Society
Published on Web 08/14/2007

solution was stored at 4 °C for 30 min, and then 70% glutaraldehyde solution was added to prepare cross-linked micelles with varying cross-linking ratios (GR). The cross-linking ratio (GR) was defined as the residual molar ratio of aldehyde group to lysine in the solution. The cross-linked PIC micelle solution was then kept at 4 °C for 30 min. In order to remove excess glutaraldehyde, the cross-linked PIC micelle solution was dialyzed against buffer. The removal of free glutaraldehyde was confirmed from the absence of aldehyde species in the dialysate, as determined by colorimetric assay using 3-methyl-2-benzothiazolinone hydrazone. Then, $NaBH_3CN$ was added to the solution to convert the Schiff base linkages to alkylamine linkages by reductive amination. The reductive amination step was also confirmed by colorimetric assay using 3-methyl-2-benzothiazolinone hydrazone.

Dynamic Light Scattering Measurements. Dynamic light scattering (DLS) measurements were carried out using a DLS-700 spectrometer (Otsuka Electronics Co., Ltd., Japan) equipped with an Ar ion laser (λ = 488 nm) at 25 °C. The detection angle was fixed at 90°. The average diameter and polydispersity index were obtained by the cumulant method, and the size distribution was obtained by histogram analysis.

Evaluation of Amidase Activity of Trypsin. The amidase activity of trypsin was evaluated using L-lysine *p*-nitroanilide as a substrate. The reaction rates of the native trypsin and trypsin incorporated into the core-cross-linked micelles were determined by monitoring the change in the absorbance at 410 nm, where the wavelength for the extinction coefficient of *p*-nitroaniline after mixing of the trypsin solution and substrate solution is 8800 cm^{-1} M^{-1}. The initial reaction rate was determined from the slope of the change in the absorbance at 410 nm during the period between 150 and 250 s after mixing.

RESULTS AND DISCUSSION

The cross-linkages in the core of PIC micelles, which were prepared from trypsin and PEG-PAA, were introduced using glutaraldehyde as cross-linking reagent for the stabilization of the micellar structure. There is known to be two types of cross-linkages in the cross-linking reaction of amine compounds by glutaraldehyde: One is the Schiff base linkage formed between the primary amino group of the Lys residue in trypsin and the aldehyde group of glutaraldehyde, and the other cross-linkage involves the formation of a quaternary pyridinium structure (see Supporting Information). We have recently confirmed the formation of the quaternary pyridinium structure for lysozyme-entrapped PIC micelles cross-linked using glutaraldehyde by spectroscopic analysis (*15*). Further, the quaternary pyridinium structure might also be formed in trypsin-entrapped PIC micelles cross-linked by glutaraldehyde. Reduction of the Schiff base and pyridinium structure using $NaBH_3CN$ as a reductant results in the formation of saturated alkylamines, further stabilizing the micelle structure due to the formation of the stable covalent bonds. The nonreacted aldehyde groups in the core-cross-linked PIC micelles were also reduced to hydroxyl groups by $NaBH_3CN$ treatment, which was confirmed by using 3-methyl-2-benzothiazolinone hydrazone as an aldehyde-detecting reagent. Figure 1 shows the size distribution of PIC micelles before and after the reductive amination. Unimodal size distribution was maintained even after this treatment. Also, the reduction process induced no change in the average diameter and polydispersity index (μ_2/Γ^2), which were determined by the cumulant analysis of dynamic light scattering measurements (69.6 nm, μ_2/Γ^2 = 0.04 for the original sample; and 68.9 nm, μ_2/Γ^2 = 0.06 for the sample after the treatment).

As an evaluation of the stabilized enzymatic function, the storage stability of the amidase activity of trypsin was studied by using L-lysine *p*-nitroanilide as a substrate. Figure 2 shows

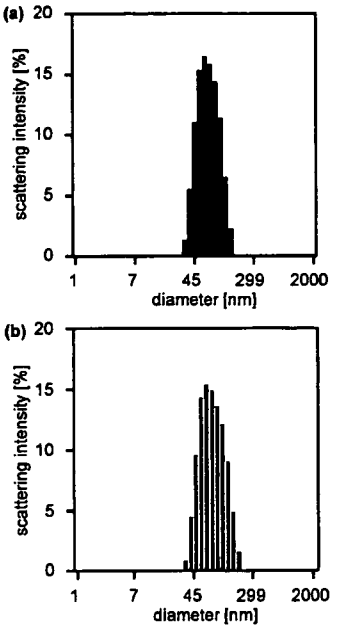

Figure 1. Size distributions of core-stabilized micelles before (a) and after (b) reductive amination, as measured by dynamic light scattering (GR = 100; detection angle 90°; temperature 25 °C).

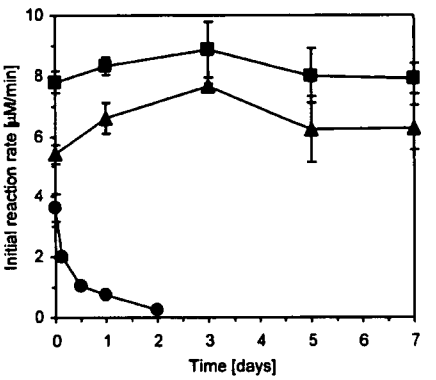

Figure 2. Time course of the enzymatic reaction rate of native trypsin (●) and trypsin incorporated into nonreduced (▲) and reduced (■) micelles at 25 °C. (Trypsin concentration 16.8 μM; substrate concentration 5 mM. The plots are presented as the average of three experiments ± SD.)

the time-dependent change in the initial reaction rate for both native trypsin and trypsin incorporated into the nonreduced and reduced micelles. The initial reaction rate of native trypsin immediately decreased due to autolysis, and there was no detectable activity after 2 days incubation. On the other hand, the trypsin incorporated into the nonreduced and reduced core-cross-linked micelles maintained a constant reaction rate even after 1 week incubation at 25 °C, indicating that the autolysis of trypsin was effectively prevented due to being incorporated into the core-cross-linked micelles. In the cross-linked core, the migration of trypsin molecules was highly restricted, thereby inhibiting their mutual contact. As a result, the autolysis of trypsin was effectively inhibited. There was no difference in the storage stability of trypsin activity between the nonreduced and reduced micelles. This effect will be discussed later on the basis of the enzymatic reaction constants. Further, it should be noted that the reaction rate of the trypsin incorporated into the core-cross-linked micelles was appreciably higher than that of native trypsin, suggesting that the amidase activity of trypsin might increase through the entrapment into the core of the